



1 Long-range transported pollution from the Middle East and its impact 2 on carbonaceous aerosol sources over Cyprus.

3 Alikı Christodoulou^{1,2}, Iasonas Stavroulas^{1,3}, Mihalis Vrekoussis^{1,4,5}, Maximillien Desservettaz¹, Michael Pikridas¹,
4 Elie Bimenyimana¹, Matic Ivančič⁶, Martin Rigler⁶, Philippe Goloub⁷, Konstantina Oikonomou¹, Roland Sarda-
5 Estève⁸, Chrysanthos Savvides⁹, Charbel Afif^{1,10}, Nikos Mihalopoulos^{1,3}, Stéphane Sauvage² and Jean Sciare¹

6

7 ¹Climate and Atmosphere Research Center (CARE-C), the Cyprus Institute, Nicosia, 2121, Cyprus

8 ²IMT Nord Europe, Institut Mines-Télécom, Univ. Lille, Centre for Energy and Environment, 59000 Lille, France

9 ³Institute for Environmental Research and Sustainable Development, National Observatory of Athens, Athens, Greece

10 ⁴University of Bremen, Institute of Environmental Physics and Remote Sensing (IUP), Germany

11 ⁵Center of Marine Environmental Sciences (MARUM), University of Bremen, Germany

12 ⁶Aerosol d.o.o., Research & Development Department, Kamniška 39a, SI-1000 Ljubljana, Slovenia

13 ⁷University of Lille, CNRS, LOA – Laboratoire d’Optique Atmosphérique, Lille, 59000, France

14 ⁸Laboratoire des Sciences du Climat et de l’Environnement (LSCE), CNRS-CEA-UVSQ, Gif-sur-Yvette, France

15 ⁹Ministry of Labour and Social Insurance, Department of Labour Inspection (DLI), Nicosia, Cyprus

16 ¹⁰Emissions, Measurements, and Modeling of the Atmosphere (EMMA) Laboratory, CAR, Faculty of Sciences, Saint Joseph

17 University, Beirut, Lebanon

18

19 *Correspondence to:* Alikı Christodoulou (a.christodoulou@cyi.ac.cy) and Jean Sciare (j.sciare@cyi.ac.cy)

20 **Abstract.** The geographical origin and source apportionment of submicron carbonaceous aerosols (organic aerosols, OA, and
21 black carbon, BC) have been investigated here for the first time by means of high time resolution measurements at an urban
22 background site of Nicosia, the capital city of Cyprus, in the Eastern Mediterranean. This study covers a half-year period,
23 encompassing both the cold and warm periods with continuous observations of the physical and chemical properties of PM₁
24 performed with an Aerosol Chemical Speciation monitor (ACSM), an Aethalometer, accompanied by a suite of various ancillary
25 off and on-line measurements. Carbonaceous aerosols were dominant during both seasons (cold and warm periods), with a
26 respective contribution of 57% and 48% to PM₁, respectively, and exhibited recurrent intense night-time peaks (>20-30 μg m⁻³)
27 during the cold period associated with local domestic heating. Findings of this study show that high concentrations of sulfate
28 (close to 3 μg m⁻³) were continuously recorded, standing among the highest ever reported for Europe and originating from the
29 Middle East region.

30 Source apportionment of the OA and BC fractions was performed using the Positive Matrix Factorization (PMF) approach and
31 the combination of two models (aethalometer model and multilinear regression), respectively. Our study revealed elevated
32 hydrocarbon-like organic aerosol (HOA) concentrations in Nicosia (among the highest reported for a European urban background
33 site), originating from a mixture of local and regional fossil-fuel combustion sources. Although air masses from the Middle East
34 had a low occurrence and were observed mostly during the cold period, they were shown to strongly affect the mean
35 concentrations levels of BC and OA in Nicosia during both seasons. Overall, the present study brings to our attention the need
36 to further characterize primary and secondary carbonaceous aerosols in the Middle East; an undersampled region characterized
37 by continuously increasing fossil fuel (oil and gas) emissions and extreme environmental conditions, which can contribute to
38 photochemical aging.

39 1. Introduction

40 At the crossroads of three continents (Europe, Africa, Asia), the Eastern Mediterranean and Middle East (EMME) region faces
41 many challenges, such as rapid population growth – with its currently 400 million inhabitants – as well as political and socio-
42 economic instabilities. Environmental conditions in the region are exceptional, with the two largest deserts worldwide (Sahara,



43 Arabian) being among the most water scarce ecosystems on the planet (Terink et al., 2013). Climate change in this region is
44 extraordinarily rapid; summer temperatures, in particular, are increasing by more than twice the global mean rate (Lelieveld et
45 al., 2014), with significant impacts especially in urban areas (Mouzourides et al., 2015). While aerosol mass loadings over the
46 EMME are dominated by desert dust, concentrations of fine particles due to anthropogenic emissions are also high (Basart et al.,
47 2009) and will likely increase with continued population growth (Pozzer et al., 2012), making anthropogenic pollution in the
48 area a leading health risk and an important climate forcer (Osipov et al., 2022).

49 Based on modelling studies, it has been also concluded that the EMME is characterized by highly favourable conditions for
50 photochemical smog and ozone (O₃) formation leading to air quality standards being drastically exceeded (Lelieveld et al., 2014;
51 Zanis et al., 2014). These enhanced concentrations of fine particulates and ozone have major human health implications,
52 contributing to premature mortality (Giannadaki, et al., 2014; Lelieveld et al. 2015), which may be further exacerbated by the
53 effects of heatwaves occurring during summer within the EMME region (Zittis et al., 2022).

54 Although data derived from satellite observations of NO₂ and SO₂ has revealed strong air pollution trends in the Middle East
55 since 2010 (Lelieveld et al., 2015a), many pollution sources are still missing in emission inventories (Mclinden et al. 2016).
56 Thus, there is a current lack of a regional approach to characterize air pollution, with in-situ observation being insufficient,
57 unavailable, or of low quality (Kadygrov et al., 2015; Ricaud et al., 2018; Paris et al., 2021), limiting the possibility to reduce
58 uncertainties in regional emission inventories and implement efficient abatement strategies.

59 Significant efforts have been put forward in recent years to characterize the atmospheric composition in-situ over Cyprus, a
60 central location of the EMME region (e.g. Kleanthous et al., 2014; Debevec et al., 2017 and 2018; Pikridas et al., 2018; Dada
61 et al., 2020; Baalbaki et al., 2021; Vrekoussis et al., 2022). In-situ ground-based PM observations have clearly shown that
62 contributions of dust to PM₁₀ over Cyprus are among the highest for the entire Mediterranean basin (Querol et al. 2009; Pey et
63 al. 2013; Kleanthous et al., 2014; Pikridas et al., 2018; Achilleos et al., 2020), during dust storm events, leading to increased
64 hospitalization, particularly attributed to cardiovascular-related diseases (Middleton et al., 2008; Tsangari et al., 2016) and short-
65 term effects associated with daily mortality (Neophytou et al., 2013). These high levels of regional particulate matter are
66 responsible for exceedances in PM₁₀ EU limits in major Cypriot cities (Querol et al., 2009). Past studies on PM trends and
67 sources highlighted the important contribution of local (urban) emissions to PM₁₀ (Achilleos et al. 2014; Pikridas et al., 2018)
68 but also showed a predominant regional pattern for PM_{2.5} with major contribution of sulphur-rich sources (Achilleos et al., 2016).
69 Based on 17 years of continuous observations of reactive gases in Cyprus, Vrekoussis et al., (2022) further confirmed the major
70 contribution of long-range transport (incl. Middle East) in the observed concentration levels of carbon monoxide (CO) and
71 sulphur dioxide (SO₂), two tracers of combustion sources.

72 Those studies have highlighted the unique location of Cyprus as a receptor site of major regional pollution hotspots, making the
73 island one of the most polluted EU member states in terms PM and O₃ concentrations; the only one impacted by long-range
74 transport of poorly-regulated air pollutants originating from Middle East countries. However, still few studies are currently
75 available to assess the contribution of regional anthropogenic emissions to PM levels in Cyprus. The filter-based chemical
76 speciation study reported by Achilleos et al., (2016) is currently the most exhaustive one and was based on 24-h integrated (PM_{2.5}
77 and PM₁₀) filter samples collected every 3 days for a period of one year (2012) in four cities in Cyprus. This study concluded
78 that Cypriot cities, like many others in Europe, are characterized by a major contribution of regional sulphate and local (urban)
79 emissions from traffic and domestic heating biomass burning.

80 Herewith, a detailed description of submicron (<1µm, PM₁) chemical composition and the further source apportionment of BC
81 and OA is presented for the first time in Cyprus. State-of-the-art on-line instrumentation (e.g. Q-ACSM, Aethalometer) were
82 deployed for the investigation of the temporal variability of aerosol composition at a location representative of the urban
83 background pollution in the capital city of Nicosia. Source apportionment of submicron organic aerosols was performed using
84 the organic fragments of the ACSM and Positive Matrix Factorization (PMF). The consistency of these results was assessed
85 against the chemical analysis of parallel filter samples and on-line measurements of external tracers. This study was extended to



86 a 6-month duration in order to cover the two main seasons of the semi-arid Eastern Mediterranean climate (short mild and wet
87 winter vs. long hot and dry summer), offering a comprehensive understanding of the daily and monthly variability of local and
88 regional sources of carbonaceous aerosols. Cold and warm periods were compared to highlight the complexity of local
89 (combustion) sources and the importance of regional ones. These results were further processed to apportion Black Carbon
90 sources in Nicosia with emphasis on local versus regional contribution.

91 **2. Material and Methods**

92 **2.1 Sampling site**

93 *Cyprus*: Cyprus is the third largest island in the Mediterranean Sea, extending approximately 240km long from east-to-west and
94 100km wide. The closest countries and their distance from the capital city of Nicosia are respectively Turkey (110km), Syria
95 (250km), Lebanon (250km), Israel (300km), Egypt (400km), Jordan (430 km), and Greece (900 km from the Greek mainland),
96 (Fig. 1a).

97 The population of Cyprus (ca. 1 million inhabitants) is rather small compared to its neighbouring countries and the rapidly
98 growing (overall 400 million) population of the region (Lelieveld et al., 2013). The main urban areas of the island shown in Fig.
99 1b, are those of Nicosia (c.a. 245,000 inhabitants), Limassol (c.a. 150,000 inhabitants), Larnaca (c.a. 50,000 inhabitants) and
100 Paphos (c.a. 35,000 inhabitants). Cyprus has a Mediterranean and semi-arid climate with two main seasons: a mild cold season
101 (from December to March) and a hot warm season lasting about eight months (from April till November). Rain occurs mainly
102 in the cold season, with the warm one being extremely dry (i.e., almost no rain between May and September)(Michaelides et al.,
103 2018).

104 *Nicosia*: Nicosia is the largest city of the island and the southeasternmost of European Union Member States' capitals. Nicosia
105 is currently partitioned in two, with a buffer zone in-between under the control of the United Nations; the southern part being
106 the capital of the Republic of Cyprus. The northern part of Nicosia (and northern part of the island) is not controlled by the
107 government of the republic of Cyprus (Resolution 550, UN security council, 1984) (Fig. 1c). Geographically, Nicosia is located
108 in the centre of the island, within the Mesaoria plain, 150 m above sea level (asl), which is delimited on its northern and southern
109 edges by two mountain ranges; the Kyrenia Range culminating at 1,024 m asl, and the Troodos Mountains culminating at 1,952
110 m asl, respectively. This topography channels winds within a more or less west-east corridor (Fig. S5) feeding the city of Nicosia
111 with long-range transported air masses from Europe, Africa, or the Middle East.

112 Measurements were performed at the Cyprus Atmospheric Observatory's Nicosia station (CAO-NIC) located at the Cyprus
113 Institute premises (Athalassa Campus; 174 m asl; 35.14N, 33.38E; Fig. 1c). The measurement site is considered as an urban
114 background site, located within a low population density residential area with no significant local pollution hotspots in its vicinity
115 (i.e., no dense road traffic, industry, commercial centers, restaurants, etc) and next to the Athalassa Forestry Park.

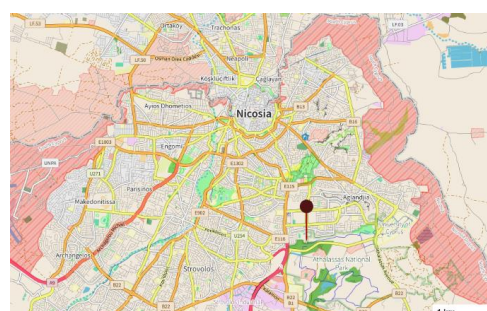
116 The period and duration of measurements presented here (07 December 2018 - 31 May 2019) were chosen to i) capture weather
117 conditions, atmospheric dynamic, and long-range pattern of the two main seasons, ii) investigate the contribution of domestic
118 heating emissions in winter, and iii) assess the potential increasing contribution of photochemical produced secondary aerosols
119 during the start of the dry and warm season. Local time (LT) in Cyprus is given as Eastern European Standard Time (EET)
120 (UTC+02:00 in winter and UTC+03:00 during the summer).



(a)



(b)



(c)

121 **Figure 1: (a) Geographic location of the island of Cyprus and its closest Northern African and Middle Eastern neighbouring countries.**
122 **(b) Location of the main cities of the Republic of Cyprus. Maps a,b were created by QGIS software v.3.26.3 utilizing the Natural Earth**
123 **data (<https://ggis.org>).** (c) **Satellite view of the Nicosia agglomeration (grey area). The buffer zone dividing the island and the city is**
124 **marked with red stripes; the location of the measurement site (CAO-NIC; The Cyprus Institute, Athalassa campus) is noted in red.**
125 **(© OpenStreetMap contributors 2022. Distributed under the Open Data Commons Open Database License (ODbL) v1.0)**

126 2.2 On-line Aerosol Instrumentation

127 On-line aerosol instrumentation has been operated following the Standard Operating Procedures defined by ACTRIS
128 (<https://www.actris.eu>), the European Research Infrastructure on Aerosols, Clouds, and Trace Gases.

129 Non-refractory submicron (NR-PM₁) aerosol chemical composition, i.e. organics, sulphate, nitrate, ammonium and chloride, was
130 continuously monitored using a Quadrupole ACSM (Aerosol Chemical Speciation Monitor; Aerodyne Research Inc.) at a 30-
131 min time resolution (Ng et al. 2011a). The instrument, along with a scanning mobility particle sizer (SMPS, described below),
132 sampled through a sharp cut cyclone operated at 4 L min⁻¹ (SCC 1.197, BGI Inc., USA), yielding an aerosol cut-off diameter of
133 approximately 1.3 μm. A nafion dryer was installed upstream, keeping sample RH below 30%. Data were retrieved using ACSM
134 local v.1.6.0.3, implemented within Igor Pro (v. 6.37, Wavemetrics Inc., USA). The ACSM is designed and built around similar
135 technology as the aerosol mass spectrometer (Jayne et al., 2000), where an aerodynamic particle focusing lens is combined with
136 particle flash vaporization in high vacuum at 600 °C, electron impact ionization, separation and final detection of the resulting
137 ions using a quadrupole mass spectrometer. Mass concentrations are calculated using a chemical composition-dependent
138 collection efficiency (Middlebrook et al., 2012).

139 Black carbon (BC) measurements were conducted using an AE-33 7-wavelength aethalometer (Magee Scientific, US) at a 1-min
140 time resolution. The aethalometer sampled ambient aerosol through a PM_{2.5} aerosol inlet (SCC 1.829, BGI Inc., USA) at a flow
141 rate of 5 L min⁻¹, after passing through a nafion dryer. The instrument internally corrected the filter loading effect in real-time,
142 while a fixed value (C₀=1.39) was applied to compensate for the multi-scattering effect (Drinovec et al., 2015). BC was
143 apportioned to source specific components, namely BC_{ff} related to fossil fuel combustion and BC_{wb} related to wood burning, by
144 applying the "aethalometer model" (Sandra Dewi et al., 2008) on the 470 – 950 nm wavelength pair, using the instrument's default



145 values for fossil fuel combustion and wood-burning aerosol Absorption Ångström Exponent, $AAE_{fr=1}$ and $AAE_{wb=2}$,
146 respectively.

147 **2.3 Ancillary measurements**

148 **SMPS:** Particle number size distributions were monitored using a scanning mobility particle sizer (SMPS) consisting of an
149 electrostatic classifier (model 3080, TSI Inc., USA) coupled with a condensation particle counter (CPC; model 3070, TSI Inc.
150 USA) operating at a 5-min time resolution and at a 1 L min^{-1} sample flow rate, measuring particles with diameter ranging from
151 9 to 700 nm. Ambient aerosols were drawn through a nafion dryer, placed upstream, keeping sample RH below 30 %. Volume
152 concentrations of assumed spherical particles derived by the SMPS were converted into mass concentrations using a variable
153 density calculated by the methodology described in Bougiatioti et al. (2014). The respective mass fractions time series of
154 chemical species were calculated based on the ACSM measurements. A density value of 1.77 g cm^{-3} was used for ammonium
155 sulphate, and 1.35 g cm^{-3} for organics (Florou et al., 2017; Lee et al., 2010), the two dominant compounds of PM_{10} in Nicosia as
156 detailed further below.

157 **Filter sampling:** Co-located 24h $PM_{2.5}$ samples were collected on quartz fiber filters (Tissuquartz, 47mm diameter, Pall) using
158 a low volume sampler (Leckel SEQ47/50) operating at a flowrate of $2.3 \text{ m}^3 \text{ h}^{-1}$. The filter samples were analysed for i) organic
159 and elemental carbon using an OC/EC Lab Instrument (Sunset Laboratory Inc., OR, USA) implementing the EUSAAR II
160 protocol (Cavalli and Putaud, 2008), ii) carbohydrates, including levoglucosan, mannosan, galactosan, using an Ion
161 Chromatography Pulsed Amperometric Detection method (Thermo - Model ICS-3000) and iii) anions (Cl^- , NO_3^- , SO_4^{2-} , MSA,
162 Oxalate) and cations (K^+ , Na^+ , NH_4^+ , Mg^{2+} , Ca^{2+}) using ion chromatography (Thermo - Model ICS-5000).

163 **Proton Transfer Reaction - Mass Spectrometry (PTR-MS):** Air was sampled through a 20m long, 3/8" o.d. (1/4" i.d.) sheathed
164 Teflon line that ran from the roof of the building to the instrument. A Teflon filter (0.2 μm diameter porosity) was installed at the
165 inlet to prevent large aerosol particles and insects from entering the sampling line. The resulting residence time of air in the line
166 was estimated to ca. 0.5 min. Temporal resolution of Volatile Organic Compounds (VOCs) measured by the PTR-MS (Ionicon
167 Analytik, Austria) was approximately two minutes (the time required to measure 55 different ions at 2 seconds per ion). The
168 basic operation principles of the PTR-MS instrument have been described in detail by Lindinger et al. (2011). Briefly, a stable
169 flow of air and high concentrations of H_3O^+ ions are continuously sampled into a drift tube held at 2.2 mbar pressure. There,
170 compounds with a proton affinity greater than water, including a large selection of Oxygenated Volatile Organic Compounds
171 (OVOCs), undergo efficient proton-transfer reactions with the H_3O^+ ions to produce protonated organic product ions, which can
172 be detected by a mass spectrometer.

173 **Meteorological Parameters:** Standard meteorological parameters (temperature, relative humidity, wind speed and direction)
174 were obtained 10 m above ground at the Athalassa Forestry Park Meteorological station of the Cyprus Department of
175 Meteorology, located at c.a. 1.3 km east from CAO-NIC station. Wind speed and direction data were further used in this study
176 for component-specific non-parametric wind regression analysis (NWR) performed using the ZeFir toolbox (Petit et al., 2017)
177 developed within the Igor Pro software (Wavemetrics Inc.). A co-located automatic CIMEL CE370 micro-LIDAR was operated
178 continuously to retrieve the Planetary Boundary Layer Height (PBLH) and better assess the influence of atmospheric dynamic
179 on in-situ ground-based observations.

180 **Air masses backtrajectory analysis:** Five-day air mass backtrajectories arriving at 1000m altitude above the sampling site were
181 computed every 6 hours, using the Hybrid Single-Particle Lagrangian Integrated Trajectory model (HYPLIT4; Stein et al., 2015)
182 using the Global Data Assimilation System (GDAS 1) meteorological data fields (with 1° spatial resolution). Backtrajectories
183 were coupled to measured concentrations, assessing origins and source contributions to specific chemical components, by
184 applying the Potential Source Contribution Function (PSCF) technique as implemented in the ZeFir toolbox described above.

185
186



187 **2.4. Source Apportionment analysis**

188 Positive Matrix Factorization (PMF) is an advanced multivariate factor analysis tool that attempts to identify the contributing
189 factors, or sources, of atmospheric pollutants at a sampling site. For this study, source apportionment was performed on the
190 organic mass spectra dataset collected by the ACSM. The (PMF) method (Paatero and Tapper, 1994) using the multilinear engine
191 (ME-2) model developed by Paatero (1999) was implemented using the SoFi (Source Finder) toolkit (SoFi 6D; Canonaco et al.,
192 2013). PMF allows the decomposition of the OA mass spectra matrix X into two matrices, G and F and a remaining residual
193 matrix E :

$$194 \quad X = G * F + E \quad (1)$$

195 Where X is the input dataset matrix (measured quantity), F is the resulting source profile matrix, G is the source contribution
196 matrix (temporal variability of each source), and E represents the model residual matrix. Based on a number of criteria the
197 optimal solution is selected, aiming at being physically meaningful that can be supported by external indicators (ancillary
198 measurements), and trying to minimize values in the residual matrix E . Model input data and error matrices (in $\mu\text{g m}^{-3}$), were
199 exported using the ACSM software. Data points with a signal-to-noise (S/N) ratio smaller than 0.2 were removed and points
200 with S/N between 0.2 and 2 were downweighted by increasing their estimated error values (Ulbrich et al., 2009; Paatero and
201 Hopke, 2003). m/z values ranging from 10 to 120 were used in the analysis. CO_2 related variables were excluded from the PMF
202 and finally reinserted in the solution.

203 Source apportionment of OA was performed following the general steps described by Crippa et al. (2014) and the recently
204 updated harmonised standard operating procedures for seasonal OA PMF (Chen et al., 2022). As a first step, unconstrained PMF
205 analyses were performed with a number of factors ranging from 2 to 8 in order to identify the most relevant number of factors
206 and potential sources. If primary organic aerosol factor profiles such as Hydrocarbon-like OA (HOA), or biomass burning-like
207 OA (BBOA) were found, then the corresponding site-specific primary OA (POA) mass spectra (see discussion below) or spectra
208 found in the literature (e.g. Ng et al., (2011) and Crippa et al., (2014)) were set as constrains in the PMF, using the “a-value”
209 approach (Paatero and Hopke, 2009; Canonaco et al., 2013). A sensitivity analysis was then performed with different a-values
210 to assess the level of constrain introduced in each factor with i) a constrained HOA using, as an anchor the HOA spectrum found
211 in Ng et al. (2011) with the a-values ranging between 0.05 and 2.0, ii) a constrained BBOA factor with the a-values from 0.2 to
212 0.5, and iii) a constrained cooking OA (COA) factor from Mohr et al. (2012) with a-values from 0.2 to 0.5. Once this sensitivity
213 analysis was completed, the evaluation of the PMF results showed that the BBOA factor could not account for the entire m/z 60
214 mass fragment, which fragment was distributed within 2 factors. Additionally, the correlation of BBOA with BC_{wb} showed to be
215 unsatisfactory (section S1). On the other hand, given the BBOA factor’s sensitivity to the type of solid fuel used, different
216 biomass burning factor profiles have been reported in various regions around the world (Mohr et al., 2012). Consequently, a site-
217 specific BBOA factor profile (BBOA_{cy}) was selected. The BBOA_{cy} spectrum was calculated as an average of 20 PMF runs from
218 the initial unconstrained PMF for the cold period, validated by it’s timeseries correlation to BC_{wb} . Since aged OA (i.e. Oxygen-
219 like OA, OOA) factors show more variability between measurement sites in terms of their mass spectra, no constrain was
220 introduced for these factors (Canonaco et al., 2015).

221 In this study, the BBOA factor - a major contributor of OA during winter - could not be properly resolved when performing the
222 PMF analysis on the entire period dataset. A seasonal approach was followed instead, separating the OA dataset into two periods
223 that were then used to describe both the two periods (cold and warm respectively). The criteria used to delineate those two
224 periods are presented and discussed in the below section 3.2.

225 One factor was consequentially constrained with the resulting BBOA_{cy} spectrum (with an a-value in the 0-0.5 range, using steps
226 of 0.02), obtaining the optimal solution using an a-value equal to 0.46. A widely referred-to standard mass spectrum (Sun et al.,
227 2016; Duan et al., 2020) derived from Ng et al. (2011) was used to constrain the HOA factor, with an a-value of 0.2, thus
228 obtaining the best correlation with BC_{tr} , a tracer for traffic related emissions. A detailed description of the OA source
229 apportionment analysis can be found in section S1 in the supplementary material.



230 3. Results and Discussion

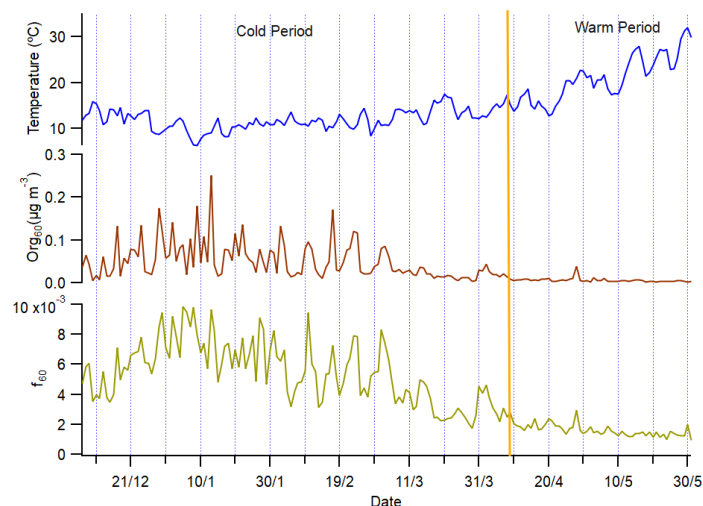
231 3.1. On-line aerosol data quality check

232 A chemical mass closure exercise for PM_{10} was performed at a temporal resolution of 1h to check the quality of the on-line aerosol
233 measurements. Chemically reconstructed PM_{10} was calculated as the sum of the mass concentration of all non-refractory species
234 measured by the ACSM (OA , NO_3^- , SO_4^{2-} , NH_4^+ , Cl^-) plus the BC concentrations measured by the Aethalometer AE-33 (Putaud
235 et al., 2004). The contribution of other chemical constituents to submicron aerosol, such as sea salt and dust (measured by co-
236 located filter sampling), was found to be low and therefore neglected here. A scatter plot of the ACSM + AE-33 measurements
237 vs the SMPS-derived PM_{10} concentrations is shown in Figure S4b. The results obtained indicate a very good correlation ($r^2 =$
238 0.88; $N=1823$) and a slope of 1.2 (Fig. S4b). This 20% discrepancy lies within the uncertainty of the on-line instruments and
239 could be attributed to the cut-off size of the SMPS at 700nm that is slightly lower compared to the ACSM. In addition, ACSM
240 individual chemical species were compared with co-located off-line analyses performed on daily $PM_{2.5}$ filters. As shown in Fig.
241 S4c-f, very good agreement was obtained between on-line and off-line measurements with $r^2 \geq 0.80$ ($N=165-175$) for all species.
242 The discrepancy between ACSM and filter measurements for nitrate (slope of 1.3) could potentially be attributed to the
243 volatilization of HNO_3 from the filter surface due to the presence of semi-volatile ammonium nitrate. The obtained slopes for
244 ammonium and sulfate below 1:1 (0.81 and 0.85, respectively) is consistent with the fact that fine $(NH_4)_2SO_4$ aerosols, mainly
245 originating from secondary processes and long-range transport (Sciare et al., 2010; Freutel et al., 2013), can be found at a large
246 size mode possibly exceeding 1 μm , consequently not being sampled by the ACSM. A very striking result obtained from the
247 comparison of OA (ACSM) with OC (from filters) is an OM-to-OC ratio of 1.42 which is at the lower end of ratios reported for
248 urban environments, which usually exhibit typical values of 1.6 ± 0.2 (Petit et al., 2015; Theodosi et al., 2011; Brown et al.,
249 2013). This low ratio clearly denotes a major contribution of long-chain hydrocarbon OA that often refer to primary combustion
250 (poorly oxidized) OA. As such, this ratio will represent a valuable and independent means of verification of the consistency of
251 our source apportionment between primary and secondary OA.

252 Finally, black carbon concentrations derived from light absorption measurements (Aethalometer AE-33) were compared against
253 filter-based EC measurements (see Fig. S4a). Data from the two techniques correlate very well ($r^2=0.83$) with a BC/EC ratio of
254 1.67 being similar to studies in other urban areas (Rigler et al., 2020; Liu et al., 2022), highlighting the existence of a BC
255 absorption enhancement (E_{abs}) attributable to a lensing effect induced by other chemical species, among which secondary OA
256 may play an important role (Zhang et al., 2018).

257 3.2 Meteorological conditions

258 **Delineation of cold vs warm seasons:** The ACSM organic mass at m/z (mass-to-charge ratio) 60 is characteristic of the
259 fragmentation of levoglucosan, a product of cellulose pyrolysis and well-established biomass burning marker (Alfarra et al.,
260 2007). Its respective contribution to total OA (f_{60}) was used in this study as an indicator of biomass burning for domestic heating
261 to delineate cold vs. warm seasons, comparing with the 0.3% threshold proposed by Cubison et al., (2011) for air masses
262 influenced by biomass burning. Except for a single small peak in early May, corresponding to open fires for the celebration of
263 the Greek Orthodox Easter, the last instance when f_{60} was above the threshold was recorded during the first week of April (Fig.
264 2). From then onwards, daily air temperature started rising constantly, from ca. 15°C in the beginning of April up to 30°C at
265 the end of May. These two features dictated the division of the dataset into two periods: a cold period of four months (07/12/2018-
266 08/04/2019), with an average temperature of $12 \pm 4^\circ C$, and a warm period of two months (09/04/2019 – 31/05/2019), with an
267 average temperature of $20 \pm 7^\circ C$.



268

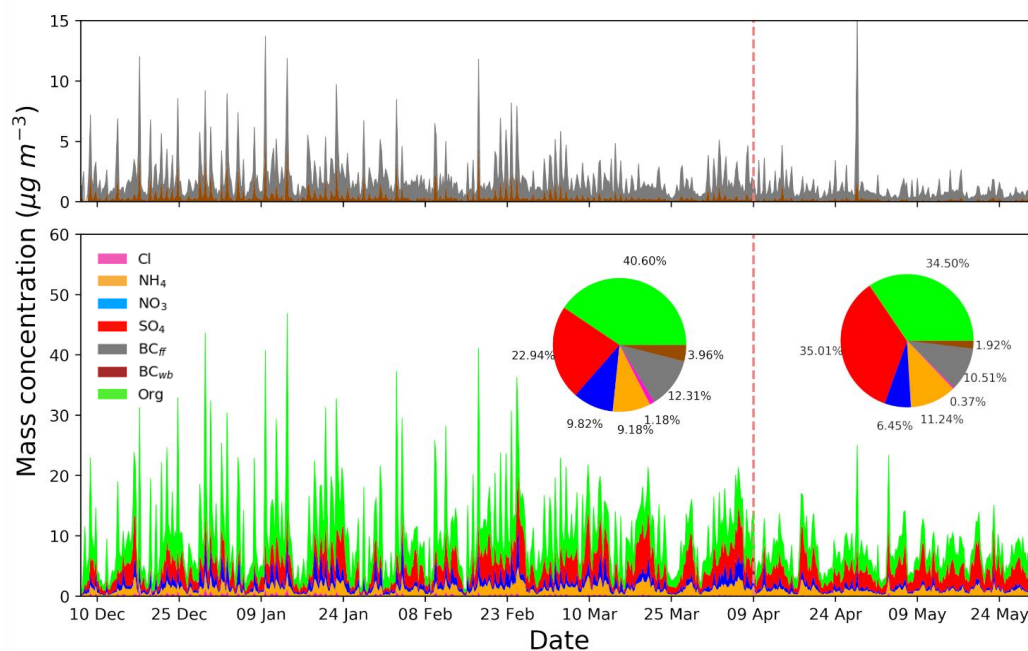
269 **Figure 2:** Time series of air temperature (blue), m/z 60 organic concentration (org60, brown) and f_{60} fragment (green) for the cold and warm
270 periods. The vertical line is used to delineate the measurements within the two seasons.

271 **Wind sectors:** During these two periods a distinct pattern in the wind sectors and the air masses arriving at the sampling site
272 was observed. As seen in Fig. S5, the dominant wind direction for the cold period was the NW-SW [225 ° - 315 °] sector
273 encompassing 48% of the total wind directions while the NE-SE [45 ° - 135 °] sector covered 26%. During the warm period the
274 weight of this proportion is shifting even more towards the NW-SW [225 ° - 315 °] sector having a 62% of total air masses while
275 only 17% are arriving from the NE-SE [45 ° - 135 °] sector.

276 **Air mass origin:** A cluster analysis was performed (Fig. S6) for both periods in order to better assess the main upwind regions
277 responsible for long-range transported air pollution over Cyprus and their change relative to the period of the year. Most of the
278 air masses arriving in Cyprus were found to originate from Europe; many of them passing over Turkey before reaching Cyprus.
279 Interestingly, this analysis showed one cluster arriving from Middle East for the cold period, whereas there were not enough
280 trajectories passing over the Middle East to calculate a cluster for this area during the warm period.

281 3.3. Chemical composition of PM₁

282 **Seasonal perspective of PM₁:** Time series of PM₁ chemical composition derived from the ACSM (OA, SO₄²⁻, NH₄⁺, NO₃⁻, Cl⁻)
283 and the Aethalometer (BC_{fit}, BC_{wb}) are depicted for the entire measuring period in Figure 3. Averaged data (6h averaging period)
284 are shown here for clarity. Furthermore, the relative average contribution of each chemical constituent to total PM₁
285 concentrations, is depicted in the respective inserted pie charts for both periods.



286

287 **Figure 3:** Time series of the chemical composition of PM₁ in Nicosia derived from 6-hour averages of ACSM and AE-33 measurements. The
288 vertical dashed red line separates the cold from the warm season. The average relative contribution of each species is shown in the respective
289 pie charts (inner panels) for each season.

290 Although intense and short duration peaks are observed for carbonaceous aerosols (OA, BC_{ff}, BC_{wb}), background NR-PM₁
291 concentration levels (between peak values) remain well below 10 µg m⁻³ for the 6-h average in both seasons. In other words, no
292 PM₁ pollution episodes (with e.g. concentrations above 10 µg m⁻³) lasting for consecutive days were observed. Such lack of
293 intense and persistent PM₁ pollution episodes differs from what is reported in central and northern Europe, where stagnant
294 (anticyclonic) conditions occur together with continental (polluted) air masses, mainly in winter and springtime (e.g. Petit et al.,
295 2015). This suggests that the relatively low emissions from Cyprus (compared to the neighboring countries) together with its
296 remote marine location (i.e. far from densely populated areas) may prevent the build up of high PM₁ pollution events over
297 Nicosia. On the other hand, clear differences can be observed between both periods, with significantly higher PM₁ concentrations
298 during the cold period, associated with repeated intense peaks of OA and BC - not observed during the warm season - and
299 suggesting local combustion emissions. The highest PM₁ concentrations were observed between December 28th 2018 and January
300 13th 2019 (Fig. 3) and were associated with low temperatures and Christmas holidays, both likely to promote the use of domestic
301 heating. During the warm period, higher contribution of sulfate, and lower contribution of OA, are clearly noticeable. The
302 contribution of nitrate during the warm period, most probably in the form of semi-volatile NH₄NO₃, remains marginal, possibly
303 due to non-favourable thermodynamic conditions preventing its formation and accumulation.

304 **PM₁ chemical composition:** For the cold period, the average calculated mass concentration of PM₁ (calculated as the sum of
305 chemical components measured by AE33 and ACSM) was 12.32 ± 9.77 µg m⁻³, with 10.30 ± 7.92 µg m⁻³ being the average
306 concentration of the non-refractory species (Table 1). OA constitutes the larger fraction of PM₁ mass, with an average
307 concentration of 5.03 ± 5.48 µg m⁻³ (41 %), followed by sulfate (23 %), black carbon (16 %), nitrate (10 %), ammonium (9 %),
308 and chloride (3 %). These concentrations and the overall distribution of chemical components in NR-PM₁ are quite similar to
309 those measured by ACSM in other European cities (Bressi et al., 2021). Concentrations appear to decline during the warm period,
310 with an average calculated PM₁ concentration of 8.18 ± 4.65 µg m⁻³, including 7.15 ± 3.80 µg m⁻³ from the non-refractory



311 components. The dominant species during the warm period were sulfate and OA, each representing 35 % of PM₁, followed by
 312 black carbon (12 %), ammonium (11 %) and nitrate (6%). During that period, chloride concentrations were negligible,
 313 contributing less than 1 % (Table 1).

314 **Table 1: Species mean, standard deviation, median concentrations and respective contribution to PM₁ during cold and warm periods**
 315 **in Nicosia.**

$\mu\text{g m}^{-3}$	Cold Period				Warm Period			
	Mean	Std	Median	Contribution (%)	Mean	Std	Median	Contribution (%)
OA	5.03	5.48	3.35	40.81	2.83	1.91	2.51	34.57
SO₄²⁻	2.81	1.89	2.60	22.83	2.87	1.50	2.61	35.08
NO₃⁻	1.22	1.25	0.75	9.87	0.53	0.56	0.34	6.46
NH₄⁺	1.14	0.77	1.01	9.25	0.92	0.55	0.84	11.30
Cl⁻	0.31	0.25	0.23	2.53	0.05	0.11	0.02	0.62
BC	2.01	2.31	1.26	16.33	1.01	1.46	0.66	12.36
PM₁	12.32	9.77	10.01	100.00	8.18	4.65	7.53	100.00

316

317 Interestingly, sulfate concentrations recorded in Nicosia are much higher compared to what is commonly observed in other
 318 European countries and Mediterranean cities (Table 2) and likely reflect a regional pattern of sulfur-rich emissions compared to
 319 Europe where SO₂ emissions have strongly decreased during the last decades (Smith et al., 2011; Chin et al., 2014) thanks to the
 320 implementation of specific abatement measures on reducing sulfur emissions (European NEC Directive (EU, 2016) and United
 321 Nation Gothenburg (1999) protocol). More specifically, the importance of sulfur emissions in Turkey (2 455 Gg, EEA 2021)
 322 which were 50% higher compared to the total SO_x emissions of the EU 28 in 2019, together with the fact that half of air masses
 323 reaching Cyprus are passing over Turkey (see Fig. S6) are key contributors to the high concentrations of sulfate in our study.

324 **Table 2: Comparison of concentration, and percentage contribution to PM₁, between the main submicron chemical species derived by**
 325 **ACSM.**

	PM ₁	OA	SO ₄ ²⁻	NH ₄ ⁺	NO ₃ ⁻	Cl ⁻	Reference
	($\mu\text{g m}^{-3}$)	($\mu\text{g m}^{-3}$)	($\mu\text{g m}^{-3}$)	($\mu\text{g m}^{-3}$)	($\mu\text{g m}^{-3}$)	($\mu\text{g m}^{-3}$)	
Nicosia Cold (DJFM)	12.32	5.03	2.81	1.14	1.22	0.31	This study
Nicosia Warm (AM)	8.18	2.83	2.87	0.92	0.53	0.05	This study
Cyprus RB* (Annual)	7.6	3.26	2.66	0.98	0.23	-	Chen et al. (2022)
European UB** (Annual)	10.6	5.3	2.0		1.9	-	Bressi et al. (2021)
S. Europe RB*** (Annual)	6.3	3.5	1.3		0.8	-	Bressi et al. (2021)
Athens Winter	18.7	13.13	2.4		1.8	0.14	Stavroulas et al. (2019)
Athens Spring	6.42	3.3	2.1	0.6	0.4	0.02	Stavroulas et al. (2019)
Marseille Winter	11.9	6.17	1.12	0.86	1.58	0.09	Chazeau et al. (2021)
Marseille Spring	8.09	3.86	1.06	0.70	1.13	0.04	Chazeau et al. (2021)
Barcelona (Annual)	9.85	4.10	1.70	1.05	1.35	0.06	Via et al. (2021)

326 * Cyprus Regional background

327 ** European urban background = Barcelona (Spain) + London (UK) + Prague (Czech) + Tartu (Estonia) + Zurich (Switzerland)

328 ***Southern European regional background = Ersa (Corsica, France) + Finokalia (Crete, Greece)

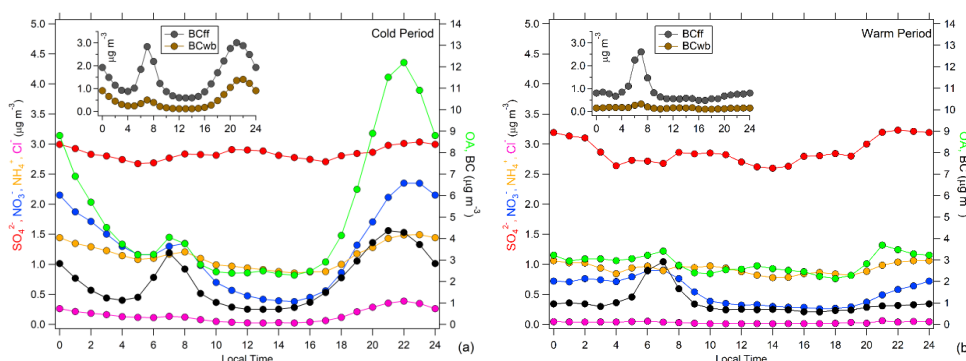
329 The main difference between the cold and warm periods lies in the decrease of concentration of carbonaceous aerosols (OA, BC)
 330 and NO₃⁻ by almost a factor of two. Several phenomena can explain this significant seasonal variation: the absence of a domestic
 331 heating source (mainly biomass burning as explained in Fig. 2); the absence of Middle East air masses during the warm period
 332 (see discussion later on); the increase in the Planetary Boundary Layer Height (PBLH) above Nicosia (Fig. S7) enhancing vertical
 333 dilution of local emissions during the warm period and therefore lowering ground-based concentrations; less favourable



334 thermodynamic conditions, with warmer and dryer air, also preventing the condensation of semi-volatile species (e.g. ammonium
335 nitrate). Sulfate concentrations do not exhibit a similar seasonal pattern and therefore seem to be less affected by the above
336 factors. On the contrary, the increase in photochemistry enhances the formation of sulfate aerosols, and the decrease in
337 precipitation enhances aerosol lifetime, strengthening the impact of long-range transport.

338 3.4. Diurnal variability of PM₁ chemical constituents

339 Figure 4 shows the diurnal variability of the PM₁ species derived from the ACSM and AE-33 for both the cold (Fig. 4a) and
340 warm (Fig. 4b) periods. The diurnal variability of the apportioned BC related to fossil fuel combustion (BC_{ff}) and wood-burning
341 (BC_{wb}) are also depicted here.



342 **Figure 4:** Diurnal variability of the main submicron chemical constituents (OA, SO₄²⁻, NO₃⁻, NH₄⁺, Cl⁻ and BC) during the a) cold and b) warm
343 periods. Diurnal profiles of BC_{ff} and BC_{wb} are embedded.

344 **Organic aerosols:** Organic aerosols clearly dominate the cold period PM₁ concentration levels, exhibiting a night-time maximum
345 above 12 µg m⁻³, and a second smaller maximum at 4 µg m⁻³ coinciding with local traffic rush hour (06:00-09:00 LT). Elevated
346 OA concentrations in the cold period during the night (max at 22:00 LT) are a common well-documented feature in many urban
347 environments across Europe and the Mediterranean (e.g. Florou et al., 2017; Stavroulas et al., 2019; Chazeau et al., 2021). They
348 can be attributed to higher emissions from domestic heating, evening traffic peak and cooking activities. The strong correlation
349 between OA and BC_{wb} (R²=0.81; N=2934; Fig. S8) suggests that residential wood burning is an important contributor to this
350 nighttime peak. Interestingly, this peak is not significantly amplified by a lower PBLH during night-time, which seems to remain
351 relatively stable with no significant diurnal variability during the cold period (Fig. S7). It is also worth noting that background
352 OA concentrations observed both at the end of the night and middle of the day, when local emissions are minimal, remain
353 relatively high at ca. 3 µg m⁻³. The diurnal variability of OA is much less pronounced during the warm period, suggesting a more
354 important contribution of regional sources to OA compared to the strong dynamic of local emissions. The assumption of a more
355 important contribution from regional OA during the warm period is further supported by a mean OA concentration of 2.83 µg
356 m⁻³ (Table 2) that is close to the averaged OA concentrations of 3.2 µg m⁻³ reported for a 2-year period continuous observations
357 with Q-ACSM (2015-2016) at the rural background site of the Cyprus Atmospheric Observatory at Agia Marian Xyliatou (CAO-
358 AMX), ca. 40km distance from Nicosia (Chen et al., 2022). During the warm period, a small OA peak remains visible in the
359 morning, with similar amplitude to the cold season, likely to be related to traffic emissions. A second peak can be observed at
360 21:00 LT (not observed in BC) which may possibly originate from cooking activities.

361 **Black carbon:** During the cold season, BC follows a bimodal diurnal pattern, which can be further apportioned by focusing on
362 its source-specific components BC_{ff} and BC_{wb}. The fossil fuel component exhibits two maxima, one in the early morning,



363 coinciding with traffic rush hour, and one in the late afternoon, most probably related to both traffic and increase in energy
364 demand due to domestic heating (see discussion later on). On the other hand, BC_{wb} diurnal variability is dominated by a night-
365 time maximum (20:00 - 01:00 LT), peaking one hour after BC_{ff} and linked to wintertime residential wood-burning emissions,
366 contributing up to 33 % of total BC. During the warm season, the BC diurnal pattern is characterised by the absence of a night-
367 time maximum, while still exhibiting a significant peak in the morning, dominated by BC_{ff} . The very low contribution of biomass-
368 related combustion particles during the warm period, as previously noted from m/z 60 in Fig. 2, is further supported here with
369 BC_{wb} exhibiting a nearly flat diurnal variability with close-to-zero mass concentrations.

370 **Secondary inorganic aerosols:** During the cold season, non-refractory nitrate and chloride detected by the Q-ACSM are mostly
371 present in the form of semi-volatile NH_4NO_3 and NH_4Cl (Guo et al., 2017; Theodosi et al., 2018). They show a night-time
372 maximum (Fig. 4-a), reflecting the presence of gas precursors (NH_3 , HNO_3 , HCl) and the more favourable thermodynamic
373 conditions with lower temperatures, higher relative humidity, and condensation sink due to high PM concentrations of
374 combustion aerosols (traffic, domestic heating). Additionally, there is a smaller morning NO_3^- peak most probably linked to
375 traffic (Foret et al., 2022). This is not observed for chloride, suggesting that HCl may not be as abundant in the morning compared
376 to the evening. The less favourable thermodynamic conditions during the warm period leads to very small concentrations of
377 semi-volatile NO_3^- and Cl^- (Fig. 4b). As expected, sulfate does not show a pronounced diurnal pattern, irrespective of the period,
378 and pointing to regionally-processed aerosols (Fig. 4a,b).

379 3.5. OA Source Apportionment

380 3.5.1 OA source apportionment during the cold period

381 For the cold period, the optimal PMF result has been found using a 5-factor solution following the approach detailed in section
382 2.4. The identification of OA sources related to these 5 factors was then performed following the typical combination of
383 information from i) OA mass spectra (Fig. S9a), ii) the correlation of each factor with source-specific tracers (see Fig. 5), iii)
384 their diurnal variability (Fig. 6a), and iv) their daily (week days vs week-end) pattern (also Fig. 6b). The five factors were then
385 assigned to the following sources: A primary BBOA (Biomass Burning Organic Aerosol), two primary HOA (Hydrocarbon-like
386 Organic Aerosol; HOA-1 and HOA-2) and two secondary OA sources, namely MO-OOA (Low-volatile Oxygenated Organic
387 Aerosol) and LO-OOA (Semi-volatile Oxygenated Organic Aerosol). This source apportionment is presented and justified below
388 for each factor:

389 **HOA-1 (Hydrocarbon-Like OA Type 1):** The mass spectrum of HOA-1 (Fig. S9a) is consistent with a fossil fuel (traffic)
390 combustion source that can be identified by the prevailing contributions of the ion series representing C_nH_{2n-1} (m/z = 27, 41, 55,
391 69, 83, 97, typical fragments of cycloalkanes or unsaturated hydrocarbon chains) and C_nH_{2n+1} (m/z = 29, 43, 57, 71, 85, 99,
392 typical fragments of alkane chains). Hence, this factor mass spectrum is well correlated to eight selected HOA factors related to
393 vehicular traffic found in the literature (Fig. S10a) and relevant to European and Mediterranean environments. The traffic-related
394 origin of the HOA-1 factor can be further confirmed by the good correlation with BC_{ff} ($R^2=0.65$; $N=2934$; Fig. S11a), benzene
395 ($R^2=0.72$; $N=1165$; Fig. S11b). The diurnal variability of HOA-1 shows a bimodal cycle with a sharp maximum during the
396 morning rush hour with an amplitude similar to BC_{ff} (Fig. 6a), and a broader maximum in the evening possibly encompassing
397 emissions from traffic and diesel fired residential heating systems. In the weekly cycle as depicted in Fig. 6b, the morning peak
398 decreases in Saturday and is nearly absent on Sunday mornings, aligned with the de-escalation of traffic emissions usually
399 observed during weekend mornings.

400

401 **BBOA (Biomass Burning OA):** The mass spectrum of the site-specific BBOA factor (reported as $BBOA_{cy}$ in section 2.4)
402 exhibits characteristic peaks at m/z 29, 60, and 73 (Fig. S9a), which are indicative of biomass burning (Crippa et al., 2014). The



403 mass spectrum is quite similar to other BBOA spectra found in the Mediterranean and Europe (Fig. S10c) with a key difference
404 here being the rather low contribution of signal at $m/z=43$. The biomass burning related origin of the factor is further confirmed
405 by the strong correlation with BC_{wb} ($R^2=0.81$; $N=2934$; Fig. S11c), benzene ($R^2=0.61$; $N=1162$; Fig. S11d) and levoglucosan
406 ($R^2=0.94$; $N=125$; Fig. S11e) a typical tracer of biomass burning (Fourtziou et al., 2017). The BBOA diurnal pattern exhibits an
407 expected well-marked night-time maximum around 22:00 LT, consistent with residential wood burning activities. This night-
408 time maximum is observed throughout the week (Fig. 6a) confirming the important role of wood burning for heating in the city.
409 Interestingly, the higher concentrations of BBOA as well as BC_{wb} (Fig. 6b) were observed on Sunday evenings, pointing to a
410 recreational use of fireplaces, leading to enhanced residential wood-burning emissions during the weekend, a feature also
411 reported in other sites in Europe and the US (Bressi et al., 2016; Rattanavaraha et al., 2017; Zhang et al., 2019).

412 **HOA-2 (Hydrocarbon-Like OA Type 2):** The mass spectrum obtained for this factor (Fig. S9a) is similar to the HOA-1 factor,
413 with high signals for the ion series $C_nH_{2n+1}^+$ and $C_nH_{2n-1}^+$. The main differences between these two factors occur in the relative
414 contribution of m/z 41 compared to m/z 43 and the relative contribution of m/z 55 compared to m/z 57 which are both much
415 higher for HOA-2, than for HOA-1. Furthermore, the contribution of signal to m/z 44 is more significant in HOA-2, which can
416 imply a mix of various sources and/or a possible higher degree of atmospheric processing. Other discrepancies with HOA-1
417 concern its diurnal variability with an intense maximum at night (Fig. 6a) and even more its average concentration levels, which
418 are almost three times higher than HOA-1.

419 Influence of cooking activities: The HOA-2 diurnal profile has a small peak at 13:00 LT and a significantly higher one at 21:00
420 LT effectively coinciding with typical meal times in Cyprus as well as those reported in literature for Greece (Siouti et al., 2021),
421 therefore indicating the influence of cooking activities to this factor. When plotting f_{55} vs f_{57} (Mohr et al., 2012) and colouring
422 the data points by the corresponding time of day, a distinct pattern appears with data of higher f_{55} over f_{57} being clustered to the
423 top left of the triangle, close to the fitted lines representing cooking (Fig. S12) and coinciding with midday and evening hours.
424 The night-time maxima pattern is consistent throughout the week, with the higher concentrations being recorded on Friday and
425 Saturday evenings (Fig. 6b), in line with an expected food service sector activity increase as part of Nicosia inhabitants' leisure
426 in the weekend. The mass spectrum of HOA-2, even though left unconstrained, is highly correlated to COA found in other studies
427 (Fig. S10b) in both Mediterranean and continental European urban environments. Additionally, the non-negligible signal at
428 $m/z=60$ points to the widely spread habit of meat charbroiling (Kaltsonoudis et al., 2017).

429 Influence of power plant emissions: A closer look at the diurnal variability of the HOA-2 factor shows a certain persistence of
430 this factor throughout the day, even when cooking activities are more or less absent (Fig. 6a). Such pattern could imply the
431 influence of other combustion sources, not necessarily of local origin. The influence of other combustion sources would also
432 help to explain why HOA-2 average concentrations are roughly 3 times higher than OA related to traffic (HOA-1), as it is very
433 unlikely that cooking activities can contribute solely to the observed HOA-2 concentrations. A possible contributing source could
434 be related to the energy production sector in the island which relies exclusively on heavy fuel oil. In a recent study, Vrekoussis
435 et al. (2022), utilizing satellite observations, have identified that power plants located to the North (Tekneçik powerplant, PP4,
436 362MW), North-East (Kaleçik powerplant, PP5, 153MW) and South-East (Dhekelia power station, PP3, 460MW) of Nicosia at
437 22 km, 60 km and 38 km, respectively, are significantly contributing to columnar NO_2 concentrations over the island. The
438 importance of these emission hotspots, along with their location on the island, during both the cold and warm periods is illustrated
439 in Fig. S13 and show, in particular for the Northern power plants (PP4, PP5), emissions as high as the traffic-related NO_2 over
440 Nicosia. Interestingly, in a source apportioning study on VOCs performed at the Cyprus Atmospheric Observatory – Agia
441 Marina Xyliatou (CAO-AMX), a rural remote site 32 km southwest of Nicosia, Debevec et al. (2017) have resolved a factor
442 related to industrial activity/power generation, exhibiting a connection with winds arriving from the wider eastern sector.

443 In order to assess the possible influence of Cypriot power plant emissions, the coupling of wind velocity, wind direction with
444 the HOA-2 timeseries was performed through NWR analysis (Fig S14b). This analysis highlights the association of stagnant
445 conditions (low wind speed / low dispersion) with high HOA-2 concentrations (i.e. night-time peaks) pointing to a more local



446 origin for this OA source. On the other hand, different features appear when wind velocities are higher, showing emissions
447 originating from the NW and the E-NE sectors; i.e. downwind of power plants PP4, and PP5, although long-range transport
448 influence cannot be ruled out. This is illustrated by the NWR of sulfate (Fig. S14f) which shows a dominant E sector likely to
449 originate from regional emissions. Given the positioning of the sampling site, close to the edge of Nicosia urban fabric, with the
450 Athalassa park lying to the east, such an observation can suggest transport of plumes from the operating powerplants, namely
451 PP5 and PP3 to the city. Interestingly, a similar, yet even clearer image stands for SO₂ concentrations – only half of which are
452 considered to be of urban origin (Vrekoussis et al., 2022) – measured at a suburban background site (NicRes) and a traffic site
453 (NicTra) in the city (Fig. S14g-h), with elevated SO₂ concentrations being related to eastern winds of higher velocity, further
454 corroborating that power generation related polluted plumes, traveling through the Mesaoria plain arriving to Nicosia can
455 contribute to the HOA-2 factor.

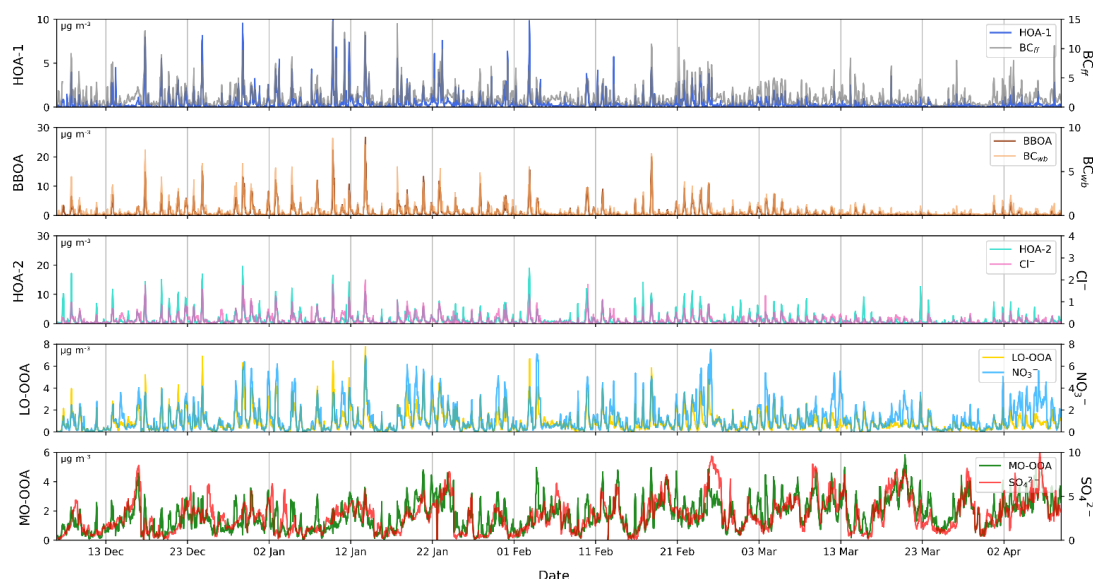
456 Other combustion sources: Interestingly, chloride shows a good correlation with HOA-2 ($r^2=0.61$; $N=2945$; see Fig. S11f, Fig.
457 5). Chloride detected by the ACSM is in the form of NH₄Cl (a secondary highly-volatile species). The source of this chloride is
458 still widely debated and may originate from industrial activity or municipal (plastic-containing) waste burning (Gunthe et al.,
459 2021). Another possible explanation of the good agreement between HOA-2 and chloride would be the use of Cl-rich coal as a
460 means for outdoor cooking in Nicosia could therefore reflect the influence of cooking activities that comprises a fraction of the
461 HOA-2 factor.

462 **Less-Oxidized Oxygenated OA (LO-OOA):** With elevated contribution of m/z 44, the mass spectrum of this factor is consistent
463 with a secondary OOA source. A higher m/z 43, and a lower m/z 44 (Fig. S9a) compared to MO-OOA, implies a less oxygenated
464 (less-processed) component (Mohr et al., 2012). Finally, the time series of this factor is quite similar to NO₃⁻, with an overall
465 good correlation value ($R^2 = 0.67$, $N=2943$; Fig. S11h) highlighting its semi-volatile character. This is further corroborated by
466 the very good correlation of LO-OOA with chloride ($R^2 = 0.73$, $N=2943$; Fig S11i), another semi-volatile compound measured
467 by the Q-ACSM. The diurnal variation of LO-OOA displays 1.5 times higher concentrations during the night compared to
468 daytime (maximum of $1.84 \pm 0.31 \mu\text{g m}^{-3}$ at 22:00 LT; Fig. 6a); a pattern that is much more pronounced than the variability
469 observed for MO-OOA. This feature highlights the fact that the presence of LO-OOA, is not exclusively controlled by
470 photochemical processes. Instead, changes in thermodynamic equilibrium (due to lower T and increased RH), favouring the
471 condensation of gas-phase semi-volatile material on one hand, and intense night-time chemistry (gas phase or heterogenous) on
472 the other hand, are among the processes that may account for the rapid night-time formation of LO-OOA. Atmospheric
473 processing of biomass burning OA during periods of low photochemical activity (such as in winter or at night), known also as
474 “dark” aging, have been reported recently (Kodros et al., 2020; Jorga et al., 2021) and could have contributed to the observed
475 night-time formation of LO-OOA. Notably, the weekly cycle of LO-OOA, and its night-time maxima, appears to have the same
476 pattern and intensity as those observed for BBOA (e.g., low peaks on Tuesday/Thursday, maximum on Sunday) (Fig. 6b). On
477 the other hand the factor is correlated with both BBOA ($R^2=0.81$; Fig. S11k) and BC_{wb} ($R^2=0.66$; Fig. S11j). This observation
478 could indicate a biomass burning contribution to LO-OOA, through fast oxidation of primary emissions, supported in several
479 studies showing biomass burning linked OOA sources at night (Stavroulas et al., 2019; Kodros et al., 2020; Chen et al., 2021).

480 **More-Oxidized Oxygenated OA (MO-OOA):** The MO-OOA factor typically accounts for secondary organic aerosol formed
481 in the atmosphere from gas-to-particle conversion processes of VOCs and their products, as well as atmospheric ageing of
482 primary OA (Petit et al., 2015; Stavroulas et al., 2019). Numerous VOC sources can contribute to OOA but lose their mass
483 spectrum fingerprint owing to extended oxidation due to photochemical aging, which leads to enhanced signal at the m/z 44
484 fragment (CO₂⁺), a dominant tracer for OOA (Ng et al., 2011). The predominance of m/z 44 and the near absence of m/z 43 in
485 the mass spectrum of the resolved MO-OOA factor (Fig. S9a) points to highly oxidized/aged secondary OA (i.e., originating
486 from long-range transport). This is further supported by the relatively good agreement ($R^2=0.55$; $N=2943$; Fig. S11i) between
487 concentrations of MO-OOA and sulphate (Fig. 5), a species of regional origin (Sciare et al., 2003). Nevertheless, the diurnal
488 variability of MO-OOA does not closely follow sulfate showing a small increase of 20-30% every evening (Fig. 6a,b) which

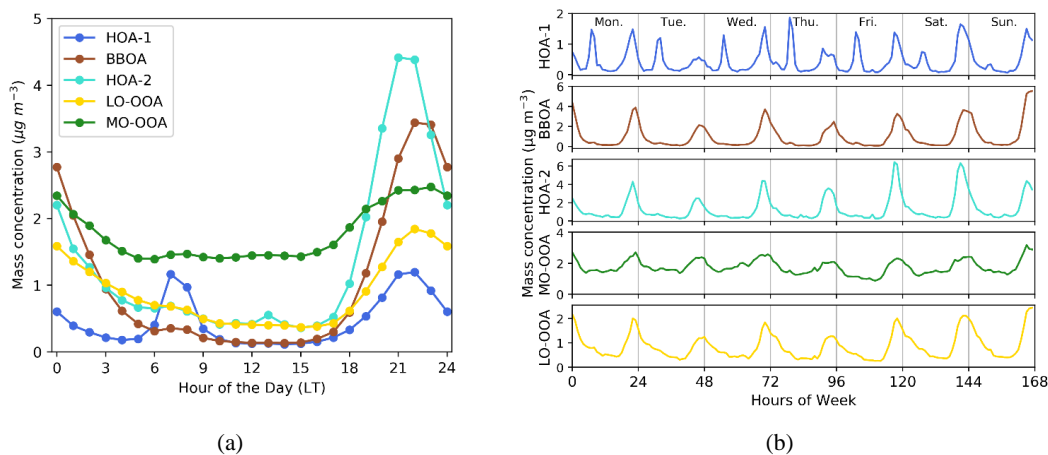


489 furthermore cannot be explained by atmospheric dynamics (c.f. the negligible PBLH diurnal variability for the cold period shown
 490 in Fig. S7). Alternatively, this would suggest that a fraction of MO-OOA is produced locally through night-time oxidation
 491 mechanisms as previously observed for LO-OOA.



492

493 **Figure 5: Time series of the five OA factors resolved along with corresponding tracer compounds for the cold period.**



494 **Figure 6: Diurnal variability (left) and weekly cycles (right) of the five OA factors averaged over the cold period..**

495 3.5.2. OA source apportionment during the warm period

496 For the warm period the optimal PMF solution was obtained using a 4-factor solution (HOA-1, HOA-2, MO-OOA, LO-OOA).
 497 As expected, the BBOA factor could not be resolved as previously highlighted by the low concentrations at m/z 60 reported
 498 during this period (Fig.2). Again, the identification of OA sources related to the 4 OA factors was performed following the
 499 typical combination of information from i) OA mass spectra (Fig. S9b), ii) the correlation of each factor with external source-
 500 specific tracers (Fig. 7 and Fig. S15), iii) their diurnal variability (Fig. 8a), and iv) their daily (week days vs week-end)
 501 pattern (also Fig. 8b). The mass spectra profiles for the 4-factor PMF solution during the warm period (Fig. S9b) were quite similar to
 502 the ones from the cold period (Fig. S9a).



503 **HOA-1:** For the warm period an α -value of 0.2 was selected for constraining the HOA-1 factor, again using the Ng et al. (2011b)
504 HOA profile as a reference. The resolved factor profile is nearly identical to the one obtained for the cold season ($R^2 = 0.99$, Fig.
505 S10a) and is also very well correlated to traffic-related HOA factor profiles found in other Mediterranean (Kostenidou et al.,
506 2015; Gilardoni et al., 2016; Florou et al., 2017; Stavroulas et al., 2019) and European cities (Lanz et al., 2010; Crippa et al.,
507 2014) as depicted in detail in Fig S10a. The HOA-1 time series follows the same pattern as the corresponding traffic-related
508 HOA-1 factor reported for the cold period, showing a good correlation with BC_{fr} , ($R^2=0.62$, $N=1259$; Fig. S15a). Its diurnal
509 variability exhibits a bimodal pattern, with a typical sharp maximum in the morning (07:00 LT) and a smaller peak during the
510 evening (Fig. 8a). On a weekly basis, this diurnal variability tends to be less pronounced on Saturdays and nearly absent on
511 Sundays (Fig. 8b), reflecting reduced commuting during the weekend.

512 **HOA-2:** The HOA-2 factor still shows elevated concentrations during the warm period, close to 3 times higher compared to
513 HOA-1 (Table S2). The profile remains quite unchanged between the cold and warm periods ($R^2= 0.92$; Fig. S10b) pointing to
514 similar sources. No correlation was observed with chloride which may be expected due to unfavourable thermodynamic
515 conditions hindering NH_4Cl formation as well as the lack of significant chloride sources during this period. A night-time
516 maximum of HOA-2 is still observed when investigating the factor's diurnal variability (Fig. 8a). Furthermore, a somewhat
517 broader, compared to the cold period, maximum in the middle of the day (Fig. 8a) can also be observed. When going through
518 the weekly variability, this midday maximum is particularly well defined on Sundays (Fig. 8b), while the evening peaks of
519 Sundays and Mondays are the lowest. The above observations remain consistent with the cold period assessment, that HOA-2
520 is on one hand linked to cooking activities. For households activities are expected at noon and evenings while for restaurants,
521 activity peaks on Sunday noon and is lower on Sunday evening and Monday reflecting the fact that such businesses remain
522 closed on the first day of the week (Fig. 8b). On the other hand, the overall offset of HOA-2 observed against the HOA-1 diurnal
523 profile persists, suggesting somewhat permanent background HOA-2 concentrations that cannot be explained by cooking
524 activities alone. A contribution to this source by continuous emissions from power plants (see space-based (SP5-TROPOMI)
525 vertical columns of NO_2 during the warm period in Fig.S13d), should be sought. In addition the HOA-2 NWR plot for the warm
526 period reveals an even more significant enhancement of concentrations when moderate winds blow from the E-SE (Fig. S16b),
527 a trend also observed for SO_2 during the same period (Fig S16e,f).

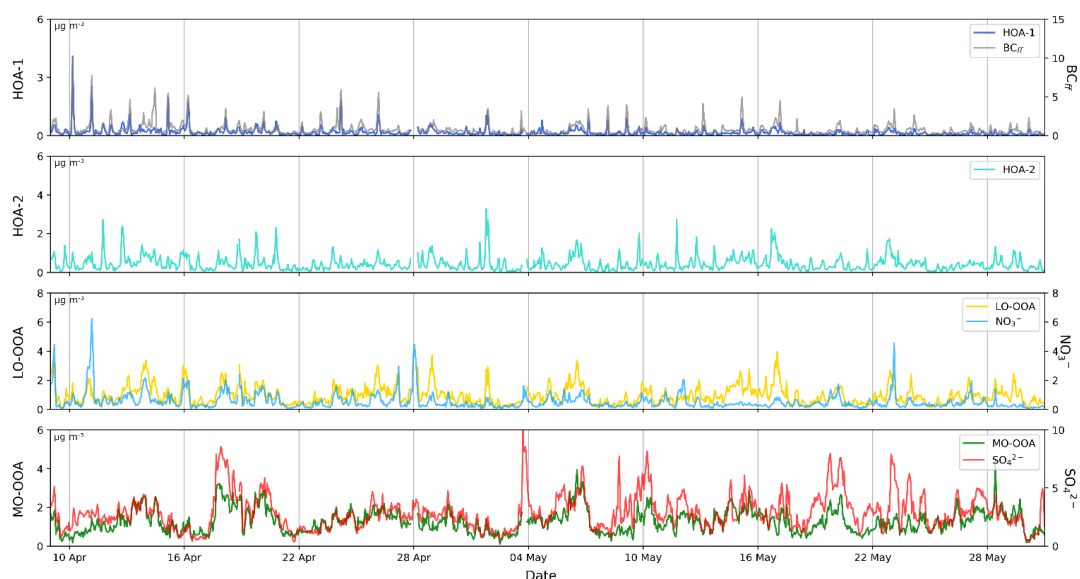
528 The above observations remain consistent with our assessment for the cold period: the HOA-2 factor consists of a mixed OA
529 source that contains cooking activities (inc. coal combustion) and emissions from the powerplants located on the eastern part of
530 the island. Indeed, the HOA-2 midday maximum can be linked to an increase in electricity demand at that time of day during the
531 warm period due to an increase in air conditioning usage (Cyprus' NECP 2021-2030, 2019).

532 **LO-OOA:** The LO-OOA factor profile exhibits some differences with the one resolved for the cold period ($R^2 = 0.66$) as
533 illustrated in the correlation matrix of comparison to selected factor profiles found in the literature (Fig. S10d) while being very
534 similar to those obtained in Athens/Piraeus during summer (Bougiatioti et al., 2014; Stavroulas et al., 2021). The LO-OOA
535 timeseries shows a low agreement with NO_3^- ($R^2 = 0.31$; $N=1259$; Fig. S15c) poorer than the observed correlation during the
536 cold period (Fig. S11h). The diurnal pattern of the factor (Fig. 8a) shows maximum concentrations persisting throughout the
537 night and early morning while a secondary maximum during midday can be observed. But overall, the diurnal pattern of LO-
538 OOA is rather flat compared to the cold period, suggesting that local production may not be so important at that time compared
539 to less variable regional background. Interestingly a midday hump similar to the one observed for HOA-2 is present, suggesting
540 a common origin.

541 **MO-OOA:** The factor profile of MO-OOA resolved during the warm period is strikingly identical to the profile found in the
542 cold period (their R^2 is almost 1; Fig. S10e), while being excellently correlated to other highly oxygenated OA factors resolved
543 in both the urban and regional background in the Eastern Mediterranean (Bougiatioti et al., 2014; Stavroulas et al., 2019, 2021)
544 as well as in continental Europe (Crippa et al., 2014). The winter night-time peaks are not observed anymore (Fig. 8a), with the
545 factor's diurnal pattern exhibiting much less variability, highlighting its dominant regional character. The time series of MO-

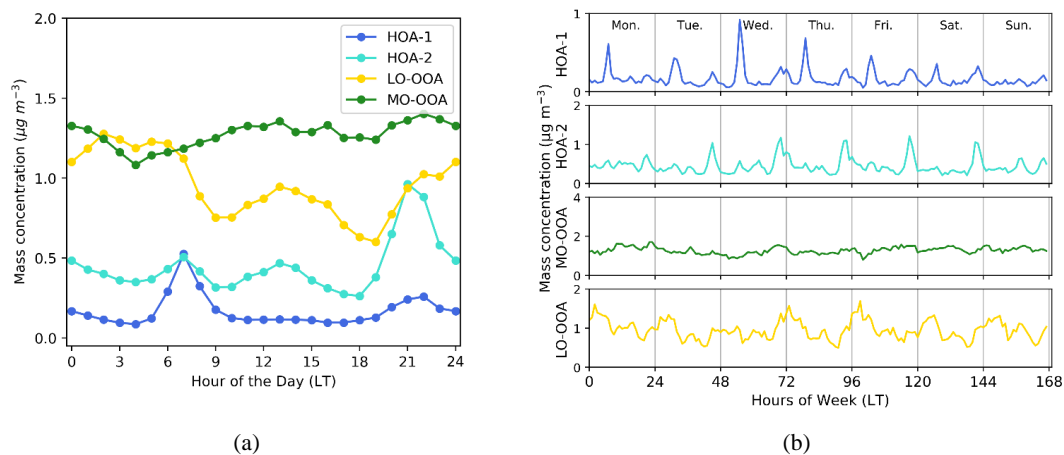


546 OOA correlates good to SO_4^{2-} ($R^2=0.53$; $N=1259$; Fig.S15b), confirming this regional and highly processed origin. The
 547 concentration levels of MO-OOA during the warm period are lower than in the cold (Table S2). However, its relative contribution
 548 to total OA during the warm period remains similar (45 %).



549

550 **Figure 7: Time series of the four OA factors resolved along with corresponding tracer compounds for the warm period.**



(a)

(b)

551 **Figure 8: Diurnal variability (a) and weekly cycles (b) of the four OA factors resolved during the warm period.**

552 3.6. Spatial and seasonal variability of OA sources

553 3.6.1. Seasonal variability of OA sources

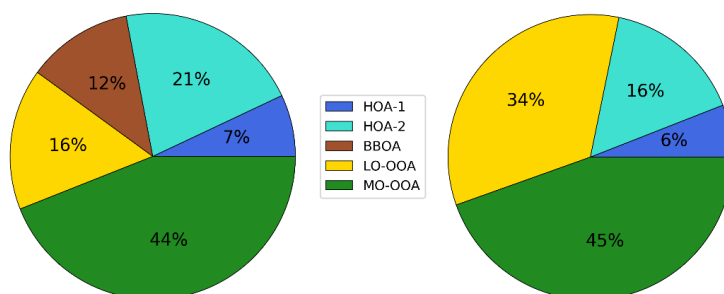
554 **Primary OA:** The mass concentration of the three primary OA factors (HOA-1, HOA-2, BBOA) represents as much as 40 % of
 555 total organic aerosols during the cold period (Fig. 9), with POA contribution significantly decreasing in the warm period (22%
 556 to total OA) due to the absence of the significant residential wood burning source which during the cold period accounted for
 557 12% of total OA. The important contribution of primary sources in Nicosia has been also highlighted earlier, by the rather low
 558 OA/OC ratio of 1.42 (Section 3.1). In a recent publication covering several European sites, Chen et al. (2022) reported that in



559 urban sites, solid fuel combustion-related OA components were 21.4 % of total OA during winter months, higher than what is
560 found for BBOA in Nicosia, owing to the rather milder winters in the city.

561 The traffic related primary factor in Nicosia (HOA-1) was found to be rather stable in terms of contribution to total OA across
562 this study's two seasons averaging 7% and 6% respectively for the cold and warm periods, being lower than the figure reported
563 in other European Urban sites (12.7%, Chen et al., 2022). On the other hand, the HOA-2 factor represents ca 2/3 of the total
564 HOA in Nicosia with little variation from winter (72 %) to summer (66 %) to total HOA (Fig. 9). Comparing it with COA in
565 urban locations resolved by Chen et al. (2022), during both winter (14.4% compared to 21% in the cold season in Nicosia) and
566 spring (15% versus 16% in Nicosia during the warm season), the higher values reported in Nicosia further support the assumption
567 that the HOA-2 represents a mixed combustion source.

568 **Secondary OA:** A higher degree of oxidation is observed for the LO-OOA factor during the warm period, given the much higher
569 contribution of signal at m/z 44 compared to the respective cold period factor. This discrepancy, reported in several studies
570 (Huang et al., 2019; Duan et al., 2020), is explained by higher photochemistry during the warm period which promotes the
571 oxidation of OA, resulting in an LO-OOA profile with a higher m/z 44 fraction. This result is also consistent with a less-oxidized
572 LO-OOA formed during the cold period from night-time chemistry. The range of LO-OOA concentration levels are different
573 between cold and warm periods (0.05-7.74 $\mu\text{g m}^{-3}$ and 0.05-4.00 $\mu\text{g m}^{-3}$, respectively), while the mean concentrations for both
574 periods are similar (0.86 and 0.95 $\mu\text{g m}^{-3}$ for cold and warm periods respectively). The contribution of LO-OOA relative to total
575 OA is double during the warm period compared to the cold, reflecting both the absence of the biomass burning source as well as
576 the prevailing conditions favoring atmospheric processing of primary OA and SOA precursors. During the cold period, LO-OOA
577 intense peaks suggest an influence from local emissions while during the warm period, the less-variable LO-OOA diurnal
578 variability highlights the influence of more intense photochemical processing at medium-to-large geographical scale. MO-OOA
579 is found to be the major contributor to total OA for both the cold (44%) and warm (45%) periods, higher in both cases than the
580 average MO-OOA contributions reported for other European urban sites (Chen et al., 2022) underlining the importance of highly
581 processed secondary OA over Nicosia (Fig. 9).



582
583 **Figure 9: Relative contribution of PMF resolved OA sources to total OA for the cold period (left) and the warm period (right)**
584 **respectively.**

585 3.6.2. Geographic origin of OA sources

586 The geographic origin of OA sources (local vs regional) is further assessed here using both Non-parametric Wind Regression
587 (NWR) analyses as well as the regional scale coupling concentrations to air mass back trajectories through PSCF.

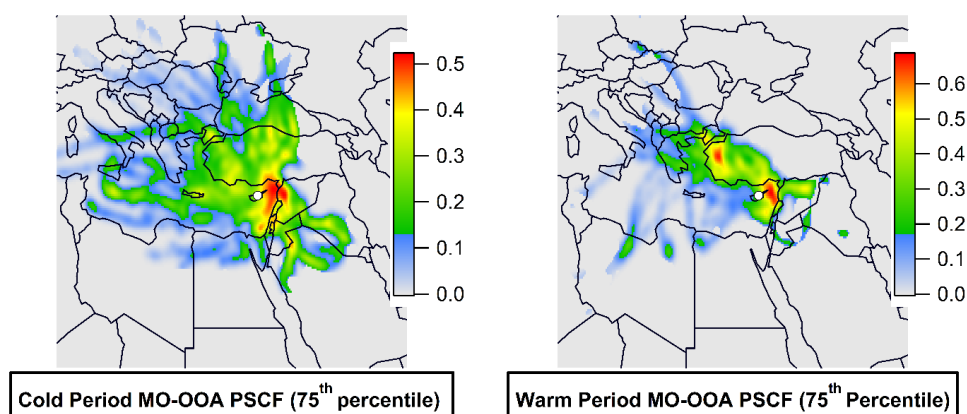
588 **Cold period:** During this period, primary OA factors, especially HOA-1 and BBOA, have an expected strong local component
589 that is characterized by high concentrations at low wind speeds (hourly average 1.4 m s^{-1}) when winds are originating from the
590 W-SW sector (Fig. S14a,c), pointing to the busy highway connecting Nicosia to the other major cities in the island while
591 integrating the highly populated residential areas of Strovolos and Lakatamia municipalities. (Fig. 1c). As discussed earlier the
592 HOA-2 factor, apart from its local influence (also in the W-SW sector), exhibits significant concentrations related to higher wind



593 speeds from the NW and the E-NE sectors that could originate from power plants but also possibly from long-range transport.
594 Interestingly, a small local contribution from the city, still within the W-SW sector, can be also observed for both LO-OOA and
595 MO-OOA, consistent with the peaks observed that could originate from local night-time chemistry. Still high concentrations of
596 MO-OOA (and to a lesser extent LO-OOA) are observed with high wind speeds and Eastern directions (Fig. S14e,d). Although
597 the contribution of the power plant PP5 located in the East sector (Fig. S13c) cannot be excluded, PSCF analysis points out that
598 the hotspots of MO-OOA can be traced in neighbouring countries (eg. Syria, Lebanon, South Turkey) in the middle East (Fig
599 10a). These areas also represent hotspots of SO_4^{2-} according to PSCF analysis (Fig. S17a).

600 **Warm period:** Given the generally higher wind speeds recorded, in comparison to the cold season (average of 1.93 m s^{-1} vs 1.36
601 m s^{-1} in the cold period), all OA factors show elevated concentrations coupled with higher wind speeds. The most striking result
602 is the major influence of the E-SE sector for all OA sources, although this sector is upwind of Nicosia and therefore poorly
603 influenced by local city emissions. As noted previously for the cold period, long-range transported OA from the Middle East is
604 expected to be the main driver here to explain the influence of the E-SE sector, at least for LO-OOA and MO-OOA (Fig. S16c,d).
605 This is once again confirmed from the PSCF results reported in Fig. 10b for the warm period. The HOA-1 factor still shows
606 maxima for low wind speeds ($<5 \text{ km h}^{-1}$) characteristic of local emissions and the SW-S direction, but also exhibits significant
607 contribution related to the E-SE sector. Although the influence of the power plant PP5 on HOA-2 is expected, contribution of
608 this source can not be exclude for HOA-1 as well. On the other hand, quantification of the Middle Eastern contribution to the
609 HOA-2 factor remains to be assessed, since the current dataset cannot provide sufficient information on separating the
610 contribution of power plants on the island versus more regional Middle East emissions (Fig. S165b). Although this hypothesis
611 needs further investigation, the presence of HOA-2 in the Middle East would be consistent with recent findings highlighting the
612 importance of OC emissions from diesel generators used in Lebanon as a mean of complementary power generation (Fadel et
613 al., 2022).

614



615

616 **Figure 10: PSCF plots for MO-OOA during the cold and warm period. Colorscale represents PSCF values while the sampling site is**
617 **denoted with a white dot .**

618 In conclusion, based on the relative contribution of OA factors (Fig. 9) and the NWR analysis (Fig. S14, S16), it can be reasonably
619 assumed that significant amount of measured OA in Nicosia is originating from long-range transport with the Middle East being
620 the major source region, during both cold and warm periods. This is the first time that such high contribution of OA from the
621 Middle East is highlighted over Cyprus. Assuming that biomass combustion and biogenic emissions of OA in the desert regions
622 of the Middle East are relatively limited, these results suggest that most of primary and secondary OA originating from the
623 Middle East could be of fossil fuel origin, which is consistent with the previously reported large use of oil in this region.



624 3.7. Spatial and seasonal variability of BC sources

625 The above conclusion on the influence of primary and secondary OA sources from the Middle East region, and its strong fossil
626 fuel origin, motivates a careful examination of the geographic origin and sources of BC concentrations recorded in Nicosia.
627 Baseline (i.e. lowest) BC_{fr} concentrations are typically observed in the middle of the night and in the middle of the day, when
628 local emissions are at their minimum (See Fig. 4). As such, these background concentrations can be considered as a first
629 qualitative indicator of background BC_{fr} concentrations of regional origin. Interestingly, these baseline BC_{fr} concentrations
630 appear to be in phase with those of sulphate (Fig. 11), as well as the MO-OOA factor derived from the OA PMF analysis. This
631 observation points to the possible use of MO-OOA as a tracer for regional BC_{fr} . Hence, it brings further evidence on the
632 importance of regional emissions on carbonaceous aerosol concentrations in Nicosia.
633

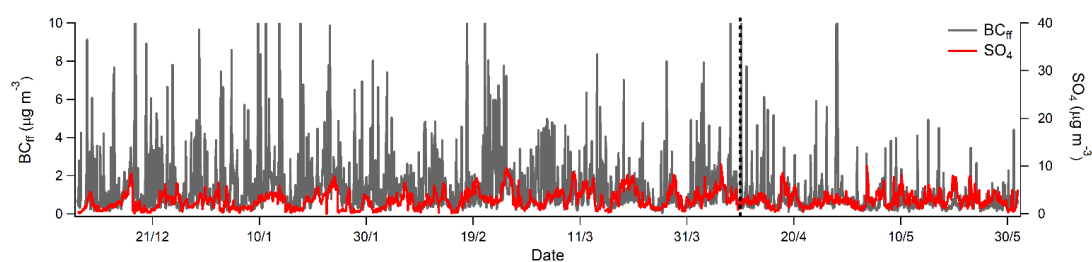


Figure 11: Temporal variability of BC_{fr} and SO_4^{2-} concentrations during the entire measuring periods.

634 The assumption that transported regional pollution can affect BC_{fr} concentrations in Nicosia can be further supported by
635 investigating the BC_{fr} NWR polar plots for both the cold and warm seasons (Fig. S18a,b). Elevated concentrations related to
636 local emissions were observed for calm conditions with low wind speeds ($<5 \text{ km h}^{-1}$) in the SW sector, as previously observed
637 for HOA-1. Interestingly, BC_{fr} NWR plots show a distinct contribution at higher wind speeds ($\sim 15 \text{ km h}^{-1}$) and the NE-SE
638 (Middle East) sector, during both the cold and warm periods, with estimated concentrations of roughly $1.5 \mu\text{g m}^{-3}$, further support
639 the major role of the Middle East in the observed BC concentration levels in Nicosia (Fig S18 a,b).

640 **BC source apportionment:** In order to better assess the relative contributions of the multiple primary OA sources (HOA-1, HOA-
641 2) and to quantify the contribution of long-range transport from the Middle East to BC_{fr} , a multilinear regression (MLR) model
642 was tentatively performed using the principle of co-emission of BC_{fr} and organic species by the different sources (Chirico et al.,
643 2010; Laborde et al., 2013). This approach, used recently by Poulain et al. (2021), assumes that at any given time (t), BC_{fr} mass
644 concentration is the sum of BC from traffic (traced by HOA-1), from a mixed combustion source (traced by HOA-2), and from
645 long-range transport (traced by MO-OOA), as follows:

$$646 \quad [BC]_{fr} = [BC]_{\text{traffic}} + [BC]_{\text{mix combustion}} + [BC]_{\text{regional}} \quad (2)$$

647 With:

$$648 \quad [BC]_{\text{traffic}} = a \times [\text{HOA-1}] \quad (3)$$

$$649 \quad [BC]_{\text{mix combustion}} = b \times [\text{HOA-2}] \quad (4)$$

$$650 \quad [BC]_{\text{regional}} = c \times [\text{MO-OOA}] \quad (5)$$

651 Where a, b, c are coefficients derived from the multi-linear regression model.

652 The above approach assumes that primary HOA-1 and HOA-2 can trace BC_{traffic} and $BC_{\text{mix combustion}}$, respectively. This is
653 somewhat expected for traffic which has a typical HOA-1/ BC_{traffic} ratio with little variations. For HOA-2, this assumption is
654 valid for the fraction that is assumed to originate from power plant emissions, and for some of the cooking activities (e.g. when
655 using charcoal combustion) but not necessarily all. As such, uncertainties of this approach is expected to be higher for HOA-2,
656 compared to HOA-1. The use of MO-OOA to trace the regional source of BC would probably lead to even higher uncertainties
657 due to the fact that MO-OOA is also sensitive to atmospheric photochemical processes and does integrate multiple sources.



658 Nevertheless, this latter assumption is believed to be acceptable given the good agreement reported above between baseline
 659 concentrations of BC_{ff} and MO-OOA (Fig. S19), and the above conclusions that carbonaceous aerosol originating from the
 660 Middle East are expected to be dominated by fossil fuel combustion. Note that MO-OOA was preferred here to LO-OOA to
 661 trace regional emissions due to the later's somewhat more local character.

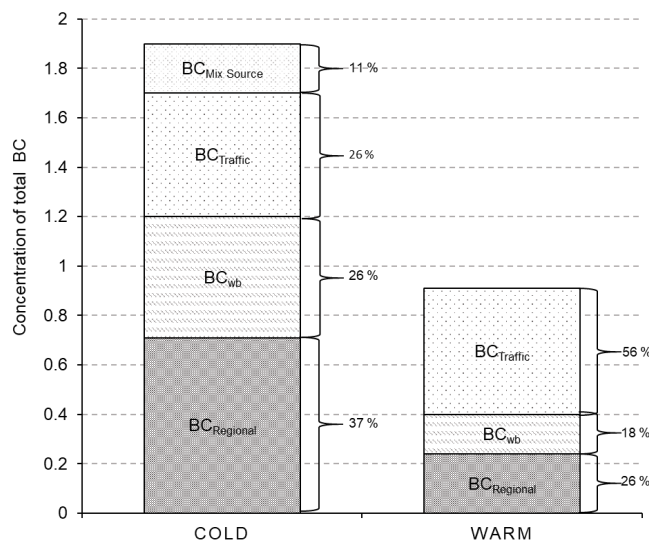
662 Combining equations 2-5 provides the multilinear regression model with the free regression parameters a , b , c which are fitted to
 663 the time-resolved BC_{ff} mass concentration measured by the Aethalometer and PMF results for the ACSM data:

$$664 \quad [BC]_{ff} = a \times [HOA-1] + b \times [HOA-2] + c \times [MO-OOA] \quad (6)$$

665 Previous studies have shown that MLR models seem to have enhanced explanatory power when primary emissions are dominant
 666 (Laborde et al., 2013). To reduce this potential bias, the MLR model was applied distinctly for the two seasons separately.

667 During the cold period, a very good correlation between measured and modelled BC_{ff} was obtained ($r^2 = 0.70$; $N = 2942$), with
 668 the modelled BC_{ff} explaining 84 % of the measured one (Fig. S20a). The regression coefficients a (HOA-1), b (HOA-2) and c
 669 (MO-OOA) were found to be 1.11 ± 0.03 , 0.15 ± 0.01 and 0.41 ± 0.01 , respectively. Regarding the warm period, it was not
 670 possible to obtain a positive value for b (HOA-2). A correlation between long-range transported HOA-2 and MO-OOA is,
 671 among other, a reason that can be proposed to explain why it has not been possible to extract a $BC_{mix\ source}$ factor here. Therefore,
 672 BC_{ff} was only apportioned using HOA-1 and MO-OOA. A good correlation between measured and modelled BC_{ff} was obtained
 673 ($r^2=0.62$; $N=1251$), with the modelled BC_{ff} , explaining 83% of observations (Fig S20b). The regression coefficients a (HOA-1)
 674 and c (MO-OOA) were found to be 3.05 ± 0.07 and 0.19 ± 0.01 , respectively.

675 The combination of the Aethalometer model (apportioning BC_{ff} and BC_{wb}) and the MLR model (apportioning $BC_{traffic}$, BC_{mix}
 676 $source$, and $BC_{regional}$) was performed to obtain an integrated picture of BC sources in Nicosia for both periods (see Fig. 12).



677
 678 **Figure 12:** BC sources during the cold and the warm period in Nicosia

679 **Spatial and seasonal variability of BC sources:** During the cold period, BC was found to originate from four different sources
 680 denoting the complexity of combustion sources of different origin in Nicosia. $BC_{regional}$ is the dominant source of BC (37%),
 681 while traffic, wood burning, and mix source are estimated to contribute to 26 %, 26% and 11% of BC, respectively. From the
 682 perspective of BC_{ff} sources, long-range transport, traced by MO-OOA, remains the largest source of BC_{ff} during the cold period,
 683 contributing 63 %, while BC_{ff} from local emissions constrained with HOA-1 and HOA-2 represents 24% and 13%, respectively
 684 (Fig S21). In other words, more than half of BC_{ff} in Nicosia was found to be regional and most probably originating from the
 685 Middle East during the cold period. This high contribution of regional BC_{ff} is quite unexpected for a medium-size European city



686 like Nicosia, where local traffic is likely to be the main contributor to BC_{fr} . Nevertheless, extra caution should be taken here and
687 the obtained contribution of 63% for BC_{fr} regional should be seen as an upper limit since a fraction of MO-OOA was shown to
688 be of local origin during the cold period. During the warm period, the picture remains similar, with traffic and wood burning
689 representing two thirds of BC (56 % & 18 %). Here, BC regional contributed 26 % to total BC. From the perspective of BC_{fr}
690 sources during warm period the long-range transport, contributed 41 %, while BC_{fr} from local emissions constrained with HOA-
691 1 represents 59 % (Fig S21). Although the two models (Aethalometer and MLR) are associated with non-negligible
692 uncertainties, the BC source apportionment obtained, shows that local emissions cannot be considered only for BC, with
693 demonstrated significant contribution of Middle East fossil fuel emissions.

694 4. Conclusions

695 Near-real-time chemical composition of submicron aerosols and source apportionment of carbonaceous aerosols was performed
696 for the first time in Nicosia, a medium-size European capital city (circa 250,000 inhabitants) in Cyprus located in the Eastern
697 Mediterranean and surrounded by Middle East countries with fast growing population and increasing emissions of air pollutants.
698 Continuous observations were performed at an urban background site, for approximately 6 months (between 7 December 2018
699 and 31 May 2019), in order to obtain a large and representative dataset capturing specific features related to cold and warm
700 periods, such as domestic heating and regional transport. Measurements of the major fractions of PM_1 were carried out with a
701 Q-ACSM and an Aethalometer complemented by a comprehensive suite of collocated instruments (e.g., filter sampling, SMPS)
702 to further assess the quality the acquired data.

703 Unlike many European cities, no clear PM_1 pollution episodes of several consecutive days could be observed over Nicosia.
704 However, very intense peaks (above $40 \mu g m^{-3}$, 1h averages) were recorded systematically every evening during the cold period.
705 Carbonaceous aerosols (BC and OA) were identified as the main components of these peaks and were mostly attributed to local
706 emissions from heating with only little contribution from local meteorology (PBL height did not show significant diurnal
707 variability during the cold period).

708 Source apportionment of OA has been used to derive a local biomass burning OA ($BBOA_{cy}$) mass spectrum, in order to properly
709 apportion the contribution of domestic wood burning. A total of five OA sources were identified during the cold period, among
710 which four are typically reported within urban environments (HOA-1, $BBOA$, LO-OOA, MO-OOA). An additional one (HOA-
711 2) was assigned as a mixture of several combustion sources such as cooking as well as a significant contribution from power
712 plants located in the Northern part of the island. These power plants in addition represent major island-based hotspots of NO_x ,
713 as evidenced from satellite observations. Interestingly, a similar HOA-2 source was identified at our regional background site
714 (40 km distance from Nicosia; Chen et al., 2022), pointing to a possible influence from these power plants to an extended part
715 of the island. The impact of this specific source brings the OA contribution of primary sources up to 40 % over Nicosia during
716 the cold period. Few additional features were noticed for the other OA sources with 1) a typical traffic-related (HOA-1) source
717 observed during both seasons, 2) a biomass burning source ($BBOA$) related to domestic heating enhanced at night during the
718 cold season and accounting for 12 % of the total OA, 3) a less oxidized secondary (LO-OOA) source of a semi-volatile character
719 and influenced by local night-time chemistry that shows to be more oxidized (and of more regional origin) during the warm
720 period, and 4) a secondary (MO-OOA) source mostly of regional origin but also influenced by night-time chemistry during the
721 cold period.

722 The geographic origin of each OA source was assessed for both seasons. With the exception of MO-OOA, which shows
723 systematically a strong regional component, HOA-1, HOA-2, and LO-OOA exhibit a clear local origin during both seasons, and
724 a more pronounced influence from the Eastern wind sector during the warm period. The prevalence of this sector is systematically
725 observed for MO-OOA highlighting the major role of Middle East emissions in contributing to ca. half of OA concentrations in
726 Nicosia during both cold and warm seasons.



727 To further elucidate the influence of this complex mixture of OA sources on BC levels, a source apportionment of BC was
728 performed combining i) the aethalometer model to separate BC into its fossil fuel (BC_{ff}) and wood burning components (BC_{wb}),
729 and ii) a multi-linear regression model to apportion the contribution to BC_{ff} from traffic (constrained by HOA-1), mix combustion
730 sources from cooking and power plants (constrained by HOA-2), and long-range transport from the Middle East (constrained by
731 MO-OOA). Although several assumptions and uncertainties are associated with this approach, it has shown to provide an
732 interesting tool to reconstruct the BC concentrations derived experimentally. Such BC apportionment performed for both cold
733 and warm seasons solidified the conclusions reached through the OA source apportionment, with almost half of BC_{ff} being of
734 regional origin with the Middle East playing an important role. This result is quite unexpected given that local traffic emissions
735 are usually considered the dominant contributor to BC_{ff} in urban background environments. These conclusions have numerous
736 implications related to PM regulation and the efficiency of local abatement strategies (in particular regarding traffic emissions),
737 health (combustion aerosols being considered as particularly adverse for human health), and climate (major influence of light
738 absorbing aerosols from Middle East fossil fuel emissions).

739 More accurate OA and BC source apportionment i) with more co-located high resolution measurements of specific trace metal
740 and organic tracers, ii) better resolved OA mass spectra (e.g., from HR-ToF-AMS), iii) the use of various source specific mass
741 spectra fingerprints (e.g., from cooking or power plants), and iv) multi-site measurements (incl. both urban and regional
742 background) will enable a more accurate estimation of local vs regional fossil fuel emissions in Cyprus while better constraining
743 the current regional efforts on air quality modelling and forecasting.

744

745 Data availability: All data used in this study can be accessed here: <https://doi.org/10.5281/zenodo.7186341>. More details on the
746 analyses are available upon request to the contact author Alikı Christodoulou (a.christodoulou@cyi.ac.cy).

747

748 Author contributions. AC, IS, MP, PG, KO, EB, RSE, MI, and MR contributed to the acquisition of measurements. AC, IS
749 contributed to the processing of the data. AC, IS and JS wrote the manuscript. MV, NM, MD, SS, MP contributed to the scientific
750 review and improvement of the manuscript. All authors have read and agreed to the published version of the manuscript

751

752 Acknowledgements.

753 This paper contains modified Copernicus Sentinel data processed at IUP Bremen. The authors thank Andreas Richter for
754 providing the TROPOMI/S5P level 1 and level 2 products. This study has been co-funded by the European Union's Horizon
755 2020 research and innovation programme under grant agreement No 615 856612 (EMME-CARE), and by the Norwegian
756 Financial Mechanism and the Republic of Cyprus under the ACCEPT project (CY-LOCALDEV-0008) in the framework of the
757 programming period 2014 – 2021.

758

759 Competing interests. The authors declare that they have no conflict of interest. At the time of the research, Matic Ivančić and
760 Martin Rigler were employed by the manufacturer of the Aethalometer.

761



762 References

- 763 Achilleos, S., Evans, J. S., Yiallourous, P. K., Kleanthous, S., Schwartz, J., and Koutrakis, P.: PM10 concentration levels at an
764 urban and background site in Cyprus: The impact of urban sources and dust storms, *J. Air Waste Manag. Assoc.*, 64, 1352–1360,
765 <https://doi.org/10.1080/10962247.2014.923061>, 2014.
- 766 Achilleos, S., Wolfson, J. M., Ferguson, S. T., Kang, C. M., Hadjimitsis, D. G., Hadjicharalambous, M., Achilleos, C.,
767 Christodoulou, A., Nisanzi, A., Papoutsas, C., Themistocleous, K., Athanasatos, S., Perdikou, S., and Koutrakis, P.: Spatial
768 variability of fine and coarse particle composition and sources in Cyprus, *Atmos. Res.*, 169, 255–270,
769 <https://doi.org/10.1016/j.atmosres.2015.10.005>, 2016.
- 770 Alfarra, M. R., Prevot, A. S. H., Szidat, S., Sandradewi, J., Weimer, S., Lanz, V. A., Schreiber, D., Mohr, M., and Baltensperger,
771 U.: Identification of the mass spectral signature of organic aerosols from wood burning emissions, *Environ. Sci. Technol.*, 41,
772 5770–5777, <https://doi.org/10.1021/es062289b>, 2007.
- 773 Basart, S., Pérez, C., Cuevas, E., Baldasano, J. M., and Gobbi, G. P.: Aerosol characterization in Northern Africa, Northeastern
774 Atlantic, mediterranean basin and middle east from direct-sun AERONET observations, *Atmos. Chem. Phys.*, 9, 8265–8282,
775 <https://doi.org/10.5194/acp-9-8265-2009>, 2009.
- 776 Borbon, A., Sauvage, S., Gouw, J. A. De, Colomb, A., Gros, V., Freutel, F., and Crippa, M.: Volatile and intermediate volatility
777 organic compounds in suburban Paris: variability, origin and importance for SOA formation, 10439–10464,
778 <https://doi.org/10.5194/acp-14-10439-2014>, 2014.
- 779 Bougiatioti, A., Stavroulas, I., Kostenidou, E., Zampas, P., Theodosi, C., Kouvarakis, G., Canonaco, F., Prévôt, A. S. H., Nenes,
780 A., Pandis, S. N., and Mihalopoulos, N.: Processing of biomass-burning aerosol in the eastern Mediterranean during summertime,
781 *Atmos. Chem. Phys.*, <https://doi.org/10.5194/acp-14-4793-2014>, 2014.
- 782 Bressi, M., Cavalli, F., Belis, C. A., Putaud, J., Fröhlich, R., Martins, S., Petralia, E., Prévôt, A. S. H., Berico, M., Malaguti, A.,
783 Bressi, M., and Belis, C. A.: Variations in the chemical composition of the submicron aerosol and in the sources of the organic
784 fraction at a regional background site of the Po Valley (Italy), 12875–12896, <https://doi.org/10.5194/acp-16-12875-2016>, 2016.
- 785 Bressi, M., Cavalli, F., Putaud, J. P., Fröhlich, R., Petit, J. E., Aas, W., Äijälä, M., Alastuey, A., Allan, J. D., Aurela, M., Berico,
786 M., Bougiatioti, A., Bukowiecki, N., Canonaco, F., Crenn, V., Dusanter, S., Ehn, M., Elsasser, M., Flentje, H., Graf, P., Green,
787 D. C., Heikkinen, L., Hermann, H., Holzinger, R., Hueglin, C., Keernik, H., Kiendler-Scharr, A., Kubelová, L., Lunder, C.,
788 Maasikmets, M., Makeš, O., Malaguti, A., Mihalopoulos, N., Nicolas, J. B., O'Dowd, C., Ovadnevaite, J., Petralia, E., Poulain,
789 L., Priestman, M., Riffault, V., Ripoll, A., Schlag, P., Schwarz, J., Sciare, J., Slowik, J., Sosedova, Y., Stavroulas, I., Teinmaa,
790 E., Via, M., Vodička, P., Williams, P. I., Wiedensohler, A., Young, D. E., Zhang, S., Favez, O., Minguillón, M. C., and Prevot,
791 A. S. H.: A European aerosol phenomenology - 7: High-time resolution chemical characteristics of submicron particulate matter
792 across Europe, *Atmos. Environ. X*, 10, <https://doi.org/10.1016/j.aeoa.2021.100108>, 2021.
- 793 Brown, S. G., Lee, T., Roberts, P. T., and Collett, J. L.: Variations in the OM/OC ratio of urban organic aerosol next to a major
794 roadway, *J. Air Waste Manag. Assoc.*, 63, 1422–1433, <https://doi.org/10.1080/10962247.2013.826602>, 2013.
- 795 Canonaco, F., Crippa, M., Slowik, J. G., Baltensperger, U., and Prévôt, A. S. H.: SoFi, an IGOR-based interface for the efficient
796 use of the generalized multilinear engine (ME-2) for the source apportionment: ME-2 application to aerosol mass spectrometer
797 data, *Atmos. Meas. Tech.*, 6, 3649–3661, <https://doi.org/10.5194/amt-6-3649-2013>, 2013.
- 798 Canonaco, F., Slowik, J. G., Baltensperger, U., and Prévôt, A. S. H.: Seasonal differences in oxygenated organic aerosol
799 composition: Implications for emissions sources and factor analysis, *Atmos. Chem. Phys.*, 15, 6993–7002,
800 <https://doi.org/10.5194/acp-15-6993-2015>, 2015.
- 801 Cavalli, F. and Putaud, J. P.: Toward a standardized thermal-optical protocol for measuring atmospheric organic and elemental
802 carbon: The eusaar protocol, *ACS, Div. Environ. Chem. - Prepr. Ext. Abstr.*, 48, 443–446, 2008.
- 803 Chazeau, B., Temime-Roussel, B., Gille, G., Mesbah, B., D'Anna, B., Wortham, H., and Marchand, N.: Measurement report:
804 Fourteen months of real-time characterisation of the submicronic aerosol and its atmospheric dynamics at the Marseille–
805 Longchamp supersite, *Atmos. Chem. Phys.*, 21, 7293–7319, <https://doi.org/10.5194/acp-21-7293-2021>, 2021.



- 806 Chen, G., Sosedova, Y., Canonaco, F., Fröhlich, R., Tobler, A., Vlachou, A., Haddad, I. El, and Prévôt, A. S. H.: Time-dependent
807 source apportionment of submicron organic aerosol for a rural site in an alpine valley using a rolling positive matrix factorisation
808 (PMF) window, 43, 15081–15101, 2021.
- 809 Chen, G., Canonaco, F., Tobler, A., Aas, W., Alastuey, A., Allan, J., Atabakhsh, S., Aurela, M., Baltensperger, U., Bougiatioti,
810 A., Brito, J. F. De, Ceburnis, D., Chazeanu, B., Chebaicheb, H., Daellenbach, K. R., Ehn, M., El, I., Eleftheriadis, K., Favez, O.,
811 Flentje, H., Font, A., Fossom, K., Freney, E., Gini, M., Green, D. C., Heikkinen, L., Herrmann, H., Kalogridis, A., Keernik, H.,
812 Lhotka, R., Lin, C., Lunder, C., Maasikmets, M., Manousakas, M. I., Marchand, N., Marin, C., Marmureanu, L., Mihalopoulos,
813 N., Jaroslaw, N., Dowd, C. O., Ovadnevaite, J., Peter, T., Petit, J., Pikridas, M., Matthew, S., Pokorn, P., Poulain, L., Priestman,
814 M., Rinaldi, M., Kazimierz, R., Simon, L., Skiba, A., Slowik, J. G., Sosedova, Y., Stavroulas, I., Styszko, K., Teinmaa, E.,
815 Timonen, H., Tremper, A., Vasilescu, J., Via, M., Vodi, P., Wiedensohler, A., Zografou, O., and Cruz, M.: European aerosol
816 phenomenology – 8 : Harmonised source apportionment of organic aerosol using 22 Year-long ACSM / AMS datasets, 166,
817 <https://doi.org/10.1016/j.envint.2022.107325>, 2022.
- 818 Chin, M., Diehl, T., Tan, Q., Prospero, J. M., Kahn, R. A., Remer, L. A., Yu, H., Sayer, A. M., Bian, H., Geogdzhayev, I. V.,
819 Holben, B. N., Howell, S. G., Huebert, B. J., Hsu, N. C., Kim, D., Kucsera, T. L., Levy, R. C., Mishchenko, M. I., Pan, X.,
820 Quinn, P. K., Schuster, G. L., Streets, D. G., Strode, S. A., and Torres, O.: Multi-decadal aerosol variations from 1980 to 2009:
821 A perspective from observations and a global model, *Atmos. Chem. Phys.*, 14, 3657–3690, [https://doi.org/10.5194/acp-14-3657-](https://doi.org/10.5194/acp-14-3657-2014)
822 2014, 2014.
- 823 Chirico, R., Decarlo, P. F., Heringa, M. F., Tritscher, T., Richter, R., Prévôt, A. S. H., Dommen, J., Weingartner, E., Wehrle, G.,
824 Gysel, M., Laborde, M., and Baltensperger, U.: Impact of aftertreatment devices on primary emissions and secondary organic
825 aerosol formation potential from in-use diesel vehicles: Results from smog chamber experiments, *Atmos. Chem. Phys.*, 10,
826 11545–11563, <https://doi.org/10.5194/acp-10-11545-2010>, 2010.
- 827 Crippa, M., Canonaco, F., Lanz, V. A., Äijälä, M., Allan, J. D., Carbone, S., Capes, G., Ceburnis, D., Dall’Osto, M., Day, D. A.,
828 DeCarlo, P. F., Ehn, M., Eriksson, A., Freney, E., Ruiz, L. H., Hillamo, R., Jimenez, J. L., Junninen, H., Kiendler-Scharr, A.,
829 Kortelainen, A. M., Kulmala, M., Laaksonen, A., Mensah, A. A., Mohr, C., Nemitz, E., O’Dowd, C., Ovadnevaite, J., Pandis, S.
830 N., Petäjä, T., Poulain, L., Saarikoski, S., Sellegri, K., Swietlicki, E., Tiitta, P., Worsnop, D. R., Baltensperger, U., and Prévôt,
831 A. S. H.: Organic aerosol components derived from 25 AMS data sets across Europe using a consistent ME-2 based source
832 apportionment approach, *Atmos. Chem. Phys.*, 14, 6159–6176, <https://doi.org/10.5194/acp-14-6159-2014>, 2014.
- 833 Cubison, M. J., Ortega, A. M., Hayes, P. L., Farmer, D. K., Day, D., Lechner, M. J., Brune, W. H., and Apel, E.: and Physics
834 Effects of aging on organic aerosol from open biomass burning smoke in aircraft and laboratory studies, 12049–12064,
835 <https://doi.org/10.5194/acp-11-12049-2011>, 2011.
- 836 Debevec, C., Sauvage, S., Gros, V., Sciare, J., Pikridas, M., Stavroulas, I., Salameh, T., Leonardis, T., Gaudion, V., Depelchin,
837 L., Fronval, I., Sarda-Estevé, R., Baisnée, D., Bonsang, B., Savvides, C., Vrekoussis, M., and Locoge, N.: Origin and variability
838 in volatile organic compounds observed at an Eastern Mediterranean background site (Cyprus), *Atmos. Chem. Phys.*, 17, 11355–
839 11388, <https://doi.org/10.5194/acp-17-11355-2017>, 2017.
- 840 Drinovec, L., Močnik, G., Zotter, P., Prévôt, A. S. H., Ruckstuhl, C., Coz, E., Rupakheti, M., Sciare, J., Müller, T., Wiedensohler,
841 A., and Hansen, A. D. A.: The “dual-spot” Aethalometer: An improved measurement of aerosol black carbon with real-time
842 loading compensation, *Atmos. Meas. Tech.*, 8, 1965–1979, <https://doi.org/10.5194/amt-8-1965-2015>, 2015.
- 843 Duan, J., Huang, R., Li, Y., Chen, Q., Zheng, Y., Chen, Y., Lin, C., and Ni, H.: Summertime and wintertime atmospheric
844 processes of secondary aerosol in Beijing, 3793–3807, 2020.
- 845 Dulac, F. and Hamonou, E.: Chapter 4. Air quality and climate in the Mediterranean region, *Mediterr. Reg. under Clim. Chang.*
846 *A Sci. Updat. Abr. English/French Version*, 39–44, <https://doi.org/10.4000/books.irdeditions.24600>, 2018.
- 847 Fadel, M., Ledoux, F., Seigneur, M., Oikonomou, K., Sciare, J., Courcot, D., and Afif, C.: Chemical profiles of PM_{2.5} emitted
848 from various anthropogenic sources of the Eastern Mediterranean: Cooking, wood burning, and diesel generators, *Environ. Res.*,
849 211, <https://doi.org/10.1016/j.envres.2022.113032>, 2022.
- 850 Florou, K., Papanastasiou, D. K., Pikridas, M., Kaltsonoudis, C., Louvaris, E., Gkatzelis, G. I., Patoulias, D., Mihalopoulos, N.,
851 and Pandis, S. N.: The contribution of wood burning and other pollution sources to wintertime organic aerosol levels in two
852 Greek cities, *Atmos. Chem. Phys.*, 17, 3145–3163, <https://doi.org/10.5194/acp-17-3145-2017>, 2017.



- 853 Foret, G., Michoud, V., Kotthaus, S., Petit, J., Baudic, A., Siour, G., Kim, Y., Doussin, J., Dupont, J., Formenti, P., Gaimoz, C.,
854 Ghersi, V., Gratién, A., Gros, V., Jaffrezo, J., Haefelin, M., Kreitz, M., Ravetta, F., Sartelet, K., Simon, L., Uzu, G., Zhang, S.,
855 Favez, O., and Beekmann, M.: The December 2016 extreme weather and particulate matter pollution episode in the Paris region
856 (France), 291, <https://doi.org/10.1016/j.atmosenv.2022.119386>, 2022.
- 857 Fourtziou, L., Liakakou, E., Stavroulas, I., Theodosi, C., Zarmpas, P., Psiloglou, B., Sciare, J., Maggos, T., Bairachtari, K.,
858 Bougiatioti, A., Gerasopoulos, E., Sarda-Estève, R., Bonnaire, N., and Mihalopoulos, N.: Multi-tracer approach to characterize
859 domestic wood burning in Athens (Greece) during wintertime, *Atmos. Environ.*, 148, 89–101,
860 <https://doi.org/10.1016/j.atmosenv.2016.10.011>, 2017.
- 861 Freutel, F., Schneider, J., Drewnick, F., Von Der Weiden-Reinmüller, S. L., Crippa, M., Prévôt, A. S. H., Baltensperger, U.,
862 Poulain, L., Wiedensohler, A., Sciare, J., Sarda-Estève, R., Burkhardt, J. F., Eckhardt, S., Stohl, A., Gros, V., Colomb, A.,
863 Michoud, V., Doussin, J. F., Borbon, A., Haefelin, M., Morille, Y., Beekmann, M., and Borrmann, S.: Aerosol particle
864 measurements at three stationary sites in the megacity of Paris during summer 2009: Meteorology and air mass origin dominate
865 aerosol particle composition and size distribution, *Atmos. Chem. Phys.*, 13, 933–959, <https://doi.org/10.5194/acp-13-933-2013>,
866 2013.
- 867 Giannadaki, D., Pozzer, A., and Lelieveld, J.: Modeled global effects of airborne desert dust on air quality and premature
868 mortality, *Atmos. Chem. Phys.*, 14, 957–968, <https://doi.org/10.5194/acp-14-957-2014>, 2014.
- 869 Gilardoni, S., Massoli, P., Paglione, M., Giulianelli, L., Carbone, C., Rinaldi, M., Decesari, S., Sandrini, S., Costabile, F., Gobbi,
870 G. P., Pietrogrande, M. C., Visentin, M., Scotto, F., Fuzzi, S., and Facchini, M. C.: Direct observation of aqueous secondary
871 organic aerosol from biomass-burning emissions, *Proc. Natl. Acad. Sci. U. S. A.*, 113, 10013–10018,
872 <https://doi.org/10.1073/pnas.1602212113>, 2016.
- 873 Gunthe, S. S., Liu, P., Panda, U., Raj, S. S., Sharma, A., Darbyshire, E., Reyes-Villegas, E., Allan, J., Chen, Y., Wang, X., Song,
874 S., Pöhlker, M. L., Shi, L., Wang, Y., Kommula, S. M., Liu, T., Ravikrishna, R., McFiggans, G., Mickleby, L. J., Martin, S. T.,
875 Pöschl, U., Andreae, M. O., and Coe, H.: Enhanced aerosol particle growth sustained by high continental chlorine emission in
876 India, *Nat. Geosci.*, 14, <https://doi.org/10.1038/s41561-020-00677-x>, 2021.
- 877 Guo, H., Liu, J., Froyd, K. D., Roberts, J. M., Veres, P. R., Hayes, P. L., Jimenez, J. L., Nenes, A., and Weber, R. J.: Fine particle
878 pH and gas – particle phase partitioning of inorganic species in Pasadena , California , during the 2010 CalNex campaign, 5703–
879 5719, <https://doi.org/10.5194/acp-17-5703-2017>, 2017.
- 880 Huang, R., Wang, Y., Cao, J., Lin, C., Duan, J., Chen, Q., Li, Y., Gu, Y., Yan, J., Xu, W., Fröhlich, R., Canonaco, F., Bozzetti,
881 C., Ovadnevaite, J., Ceburnis, D., Canagaratna, M. R., Jayne, J., Worsnop, D. R., El-haddad, I., Prévôt, A. S. H., and Dowd, C.
882 D. O.: Primary emissions versus secondary formation of fine particulate matter in the most polluted city (Shijiazhuang) in North
883 China, 2283–2298, 2019.
- 884 Jayne, J. T., Leard, D. C., Zhang, X., Davidovits, P., Smith, K. A., Kolb, C. E., and Worsnop, D. R.: Development of an aerosol
885 mass spectrometer for size and composition analysis of submicron particles, *Aerosol Sci. Technol.*, 33, 49–70,
886 <https://doi.org/10.1080/027868200410840>, 2000.
- 887 Jorga, S. D., Florou, K., Kaltsonoudis, C., Kodros, J. K., Vasilakopoulou, C., Cirtog, M., Fouqueau, A., Picquet-Varrault, B.,
888 Nenes, A., and Pandis, S. N.: Nighttime chemistry of biomass burning emissions in urban areas: A dual mobile chamber study,
889 *Atmos. Chem. Phys.*, 21, 15337–15349, <https://doi.org/10.5194/acp-21-15337-2021>, 2021.
- 890 Kadyrov, N., Broquet, G., Chevallier, F., Rivier, L., Gerbig, C., and Ciais, P.: On the potential of the ICOS atmospheric CO₂
891 measurement network for estimating the biogenic CO₂ budget of Europe, *Atmos. Chem. Phys.*, 15, 12765–12787,
892 <https://doi.org/10.5194/acp-15-12765-2015>, 2015.
- 893 Kaltsonoudis, C., Kostenidou, E., Louvaris, E., Psychoudaki, M., Tsiligiannis, E., Florou, K., Liangou, A., and Pandis, S. N.:
894 Characterization of fresh and aged organic aerosol emissions from meat charbroiling, *Atmos. Chem. Phys.*, 17, 7143–7155,
895 <https://doi.org/10.5194/acp-17-7143-2017>, 2017.
- 896 Kleanthous, S., Vrekoussis, M., Mihalopoulos, N., Kalabokas, P., and Lelieveld, J.: On the temporal and spatial variation of
897 ozone in Cyprus, *Sci. Total Environ.*, 476–477, 677–687, <https://doi.org/10.1016/j.scitotenv.2013.12.101>, 2014.



- 898 Kodros, J. K., Papanastasiou, D. K., Paglione, M., Masiol, M., Squizzato, S., Florou, K., Skyllakou, K., Kaltsonoudis, C., Nenes,
899 A., and Pandis, S. N.: Rapid dark aging of biomass burning as an overlooked source of oxidized organic aerosol, *Proc. Natl.*
900 *Acad. Sci. U. S. A.*, 117, 33028–33033, <https://doi.org/10.1073/PNAS.2010365117>, 2020.
- 901 Kostenidou, E., Florou, K., Kaltsonoudis, C., Tsiflikiotou, M., Vratolis, S., Eleftheriadis, K., and Pandis, S. N.: Sources and
902 chemical characterization of organic aerosol during the summer in the eastern Mediterranean, *Atmos. Chem. Phys.*, 15, 11355–
903 11371, <https://doi.org/10.5194/acp-15-11355-2015>, 2015.
- 904 Laborde, M., Crippa, M., Tritscher, T., Jurányi, Z., Decarlo, P. F., Temime-Roussel, B., Marchand, N., Eckhardt, S., Stohl, A.,
905 Baltensperger, U., Prévôt, A. S. H., Weingartner, E., and Gysel, M.: Black carbon physical properties and mixing state in the
906 European megacity Paris, *Atmos. Chem. Phys.*, 13, 5831–5856, <https://doi.org/10.5194/acp-13-5831-2013>, 2013.
- 907 Lanz, V. A., Prévôt, A. S. H., Alfarra, M. R., Weimer, S., Mohr, C., Decarlo, P. F., Gianini, M. F. D., Hueglin, C., Schneider, J.,
908 Favez, O., D’Anna, B., George, C., and Baltensperger, U.: Characterization of aerosol chemical composition with aerosol mass
909 spectrometry in Central Europe: An overview, *Atmos. Chem. Phys.*, 10, 10453–10471, <https://doi.org/10.5194/acp-10-10453-2010>, 2010.
- 911 Lee, B. H., Kostenidou, E., Hildebrandt, L., Riipinen, I., Engelhart, G. J., Mohr, C., Decarlo, P. F., Mihalopoulos, N., Prevot, A.
912 S. H., Baltensperger, U., and Pandis, S. N.: Measurement of the ambient organic aerosol volatility distribution: Application
913 during the Finokalia Aerosol Measurement Experiment (FAME-2008), *Atmos. Chem. Phys.*, 10, 12149–12160,
914 <https://doi.org/10.5194/acp-10-12149-2010>, 2010.
- 915 Lelieveld, J., Barlas, C., Giannadaki, D., and Pozzer, A.: Model calculated global, regional and megacity premature mortality
916 due to air pollution, *Atmos. Chem. Phys.*, 13, 7023–7037, <https://doi.org/10.5194/acp-13-7023-2013>, 2013.
- 917 Lelieveld, J., Hadjinicolaou, P., Kostopoulou, E., Giannakopoulos, C., Pozzer, A., Tanarhte, M., and Tyrllis, E.: Model projected
918 heat extremes and air pollution in the eastern Mediterranean and Middle East in the twenty-first century, *Reg. Environ. Chang.*,
919 14, 1937–1949, <https://doi.org/10.1007/s10113-013-0444-4>, 2014.
- 920 Lelieveld, J., Beirle, S., Hörmann, C., Stenchikov, G., and Wagner, T.: Abrupt recent trend changes in atmospheric nitrogen
921 dioxide over the Middle East, *Sci. Adv.*, 1, 1–6, <https://doi.org/10.1126/sciadv.1500498>, 2015a.
- 922 Lelieveld, J., Evans, J. S., Fnais, M., Giannadaki, D., and Pozzer, A.: The contribution of outdoor air pollution sources to
923 premature mortality on a global scale, *Nature*, 525, 367–371, <https://doi.org/10.1038/nature15371>, 2015b.
- 924 Liu, X., Zheng, M., Liu, Y., Jin, Y., Liu, J., Zhang, B., Yang, X., Wu, Y., Zhang, T., Xiang, Y., Liu, B., and Yan, C.:
925 Intercomparison of equivalent black carbon (eBC) and elemental carbon (EC) concentrations with three-year continuous
926 measurement in Beijing, China, *Environ. Res.*, 209, 112791, <https://doi.org/10.1016/j.envres.2022.112791>, 2022.
- 927 McLinden, C. A., Fioletov, V., Shephard, M. W., Krotkov, N., Li, C., Martin, R. V., Moran, M. D., and Joiner, J.: Space-based
928 detection of missing sulfur dioxide sources of global air pollution, *Nat. Geosci.*, 9, 496–500, <https://doi.org/10.1038/ngeo2724>,
929 2016.
- 930 Michaelides, S., Karacostas, T., Sánchez, J. L., Retalis, A., Pytharoulis, I., Homar, V., Romero, R., Zanis, P., Giannakopoulos,
931 C., Bühl, J., Ansmann, A., Merino, A., Melcón, P., Lagouvardos, K., Kotroni, V., Brüggeman, A., López-Moreno, J. I., Berthet,
932 C., Katragkou, E., Tymvios, F., Hadjimitsis, D. G., Mamouri, R. E., and Nisantzi, A.: Reviews and perspectives of high impact
933 atmospheric processes in the Mediterranean, *Atmos. Res.*, 208, 4–44, <https://doi.org/10.1016/j.atmosres.2017.11.022>, 2018.
- 934 Middlebrook, A. M., Bahreini, R., Jimenez, J. L., and Canagaratna, M. R.: Evaluation of composition-dependent collection
935 efficiencies for the Aerodyne aerosol mass spectrometer using field data, *Aerosol Sci. Technol.*, 46, 258–271,
936 <https://doi.org/10.1080/02786826.2011.620041>, 2012.
- 937 Middleton, N., Yiallourous, P., Kleanthous, S., Kolokotroni, O., Schwartz, J., Dockery, D. W., Demokritou, P., and Koutrakis, P.:
938 A 10-year time-series analysis of respiratory and cardiovascular morbidity in Nicosia, Cyprus: The effect of short-term changes
939 in air pollution and dust storms, *Environ. Heal. A Glob. Access Sci. Source*, 7, 1–16, <https://doi.org/10.1186/1476-069X-7-39>,
940 2008.



- 941 Mohr, C., DeCarlo, P. F., Heringa, M. F., Chirico, R., Slowik, J. G., Richter, R., Reche, C., Alastuey, A., Querol, X., Seco, R.,
942 Peñuelas, J., Jiménez, J. L., Crippa, M., Zimmermann, R., Baltensperger, U., and Prévôt, A. S. H.: Identification and
943 quantification of organic aerosol from cooking and other sources in Barcelona using aerosol mass spectrometer data, *Atmos.*
944 *Chem. Phys.*, 12, 1649–1665, <https://doi.org/10.5194/acp-12-1649-2012>, 2012.
- 945 Mouzourides, P., Kumar, P., and Neophytou, M. K. A.: Assessment of long-term measurements of particulate matter and gaseous
946 pollutants in South-East Mediterranean, *Atmos. Environ.*, 107, 148–165, <https://doi.org/10.1016/j.atmosenv.2015.02.031>, 2015.
- 947 Neophytou, A. M., Yiallourous, P., Coull, B. A., Kleanthous, S., Pavlou, P., Pashiardis, S., Dockery, D. W., Koutrakis, P., and
948 Laden, F.: Particulate matter concentrations during desert dust outbreaks and daily mortality in Nicosia, Cyprus, *J. Expo. Sci.*
949 *Environ. Epidemiol.*, 23, 275–280, <https://doi.org/10.1038/jes.2013.10>, 2013.
- 950 Ng, N. L., Canagaratna, M. R., Jimenez, J. L., Zhang, Q., Ulbrich, I. M., and Worsnop, D. R.: Real-time methods for estimating
951 organic component mass concentrations from aerosol mass spectrometer data, *Environ. Sci. Technol.*, 45, 910–916,
952 <https://doi.org/10.1021/es102951k>, 2011.
- 953 Osipov, S., Chowdhury, S., Crowley, J. N., Tadic, I., Drewnick, F., Borrmann, S., Eger, P., Fachinger, F., Fischer, H.,
954 Predybaylo, E., Fnais, M., Harder, H., Pikridas, M., Vouterakos, P., Pozzer, A., Sciare, J., Ukhov, A., Stenchikov, G. L.,
955 Williams, J., and Lelieveld, J.: Severe atmospheric pollution in the Middle East is attributable to anthropogenic sources,
956 *Commun. Earth Environ.*, 3, 1–10, <https://doi.org/10.1038/s43247-022-00514-6>, 2022.
- 957 Paatero, P.: The Multilinear Engine—A Table-Driven, Least Squares Program for Solving Multilinear Problems, Including the
958 n-Way Parallel Factor Analysis Model, *J. Comput. Graph. Stat.*, 8, 854–888, <https://doi.org/10.1080/10618600.1999.10474853>,
959 1999.
- 960 Paatero, P. and Hopke, P. K.: Discarding or downweighting high-noise variables in factor analytic models, 490, 277–289,
961 [https://doi.org/10.1016/S0003-2670\(02\)01643-4](https://doi.org/10.1016/S0003-2670(02)01643-4), 2003.
- 962 Paatero, P. and Hopke, P. K.: Rotational Tools for Factor Analytic Models, 91–100, <https://doi.org/10.1002/cem.1197>, 2009.
- 963 Paris, J., Riandet, A., Bourtsoukidis, E., Delmotte, M., Berchet, A., Williams, J., Ernle, L., Tadic, I., Harder, H., and Lelieveld,
964 J.: Shipborne measurements of methane and carbon dioxide in the Middle East and Mediterranean areas and the contribution
965 from oil and gas emissions, 12443–12462, 2021.
- 966 Petit, J., Favez, O., Albinet, A., and Canonaco, F.: Environmental Modelling & Software A user-friendly tool for comprehensive
967 evaluation of the geographical origins of atmospheric pollution : Wind and trajectory analyses, *Environ. Model. Softw.*, 88, 183–
968 187, <https://doi.org/10.1016/j.envsoft.2016.11.022>, 2017.
- 969 Petit, J. E., Favez, O., Sciare, J., Crenn, V., Sarda-Estève, R., Bonnaire, N., Močnik, G., Dupont, J. C., Haefelin, M., and Leoz-
970 Garziandia, E.: Two years of near real-time chemical composition of submicron aerosols in the region of Paris using an Aerosol
971 Chemical Speciation Monitor (ACSM) and a multi-wavelength Aethalometer, *Atmos. Chem. Phys.*, 15, 2985–3005,
972 <https://doi.org/10.5194/acp-15-2985-2015>, 2015.
- 973 Pey, J., Querol, X., Alastuey, A., Forastiere, F., and Stafoggia, M.: African dust outbreaks over the Mediterranean Basin during
974 2001–2011: PM10 concentrations, phenomenology and trends, and its relation with synoptic and mesoscale meteorology, *Atmos.*
975 *Chem. Phys.*, 13, 1395–1410, <https://doi.org/10.5194/acp-13-1395-2013>, 2013.
- 976 Pikridas, M., Vrekoussis, M., Sciare, J., Kleanthous, S., Vasiliadou, E., Kizas, C., Savvides, C., and Mihalopoulos, N.: Spatial
977 and temporal (short and long-term) variability of submicron, fine and sub-10 Mm particulate matter (PM1, PM2.5, PM10) in
978 Cyprus, *Atmos. Environ.*, 191, 79–93, <https://doi.org/10.1016/j.atmosenv.2018.07.048>, 2018.
- 979 Poulain, L., Fahlbusch, B., Spindler, G., Müller, K., Van Pinxteren, D., Wu, Z., Inuma, Y., Birmili, W., Wiedensohler, A., and
980 Herrmann, H.: Source apportionment and impact of long-range transport on carbonaceous aerosol particles in central Germany
981 during HCCT-2010, *Atmos. Chem. Phys.*, 21, 3667–3684, <https://doi.org/10.5194/acp-21-3667-2021>, 2021.
- 982 Pozzer, A., Zimmermann, P., Doering, U. M., Van Aardenne, J., Tost, H., Dentener, F., Janssens-Maenhout, G., and Lelieveld,



- 983 J.: Effects of business-as-usual anthropogenic emissions on air quality, *Atmos. Chem. Phys.*, 12, 6915–6937,
984 <https://doi.org/10.5194/acp-12-6915-2012>, 2012.
- 985 QGIS Development Team, 2009. QGIS Geographic Information System. Open Source Geospatial Foundation.
986 URL <http://qgis.org>
- 987 Querol, X., Pey, J., Pandolfi, M., Alastuey, A., Cusack, M., Pérez, N., Moreno, T., Viana, M., Mihalopoulos, N., Kallos, G., and
988 Kleanthous, S.: African dust contributions to mean ambient PM₁₀ mass-levels across the Mediterranean Basin, *Atmos. Environ.*,
989 43, 4266–4277, <https://doi.org/10.1016/j.atmosenv.2009.06.013>, 2009.
- 990 Rattanavaraha, W., Canagaratna, M. R., Budisulistiorini, S. H., Croteau, P. L., Baumann, K., Canonaco, F., Prevot, A. S. H.,
991 Edgerton, E. S., Zhang, Z., Jayne, J. T., Worsnop, D. R., Gold, A., Shaw, S. L., and Surratt, J. D.: Source apportionment of
992 submicron organic aerosol collected from Atlanta, Georgia, during 2014–2015 using the aerosol chemical speciation monitor
993 (ACSM), *Atmos. Environ.*, 167, 389–402, <https://doi.org/10.1016/j.atmosenv.2017.07.055>, 2017.
- 994 Ricaud, P., Zbinden, R., Catoire, V., Brocchi, V., Dulac, F., Hamonou, E., Canonici, J. C., El Amraoui, L., Massart, S., Piguet,
995 B., Dayan, U., Nabat, P., Sciare, J., Ramonet, M., Delmotte, M., Di Sarra, A., Sferlazzo, D., Di Iorio, T., Piacentino, S.,
996 Cristofanelli, P., Mihalopoulos, N., Kouvarakis, G., Pikridas, M., Savvides, C., Mamouri, R. E., Nisantzi, A., Hadjimitsis, D.,
997 Attié, J. L., Ferré, H., Kangah, Y., Jaidan, N., Guth, J., Jacquet, P., Chevrier, S., Robert, C., Bourdon, A., Bourdinot, J. F.,
998 Etienne, J. C., Krysztofciak, G., and Theron, P.: The GLAM airborne campaign across the Mediterranean Basin, *Bull. Am.
999 Meteorol. Soc.*, 99, 361–380, <https://doi.org/10.1175/BAMS-D-16-0226.1>, 2018.
- 1000 Rigler, M., Drinovec, L., Lavri, G., Vlachou, A., Prevot, A. S. H., Luc Jaffrezo, J., Stavroulas, I., Sciare, J., Burger, J., Kranjc,
1001 I., Turšič, J., D. A. Hansen, A., and Mocnik, G.: The new instrument using a TC-BC (total carbon-black carbon) method for the
1002 online measurement of carbonaceous aerosols, *Atmos. Meas. Tech.*, 13, 4333–4351, <https://doi.org/10.5194/amt-13-4333-2020>,
1003 2020.
- 1004 Sandradewi, J., Prévôt, A. S. H., Szidat, S., Perron, N., Alfarra, M. R., Lanz, V. A., Weingartner, E., and Baltensperger, U. R.
1005 S.: Using aerosol light absorption measurements for the quantitative determination of wood burning and traffic emission
1006 contribution to particulate matter, *Environ. Sci. Technol.*, 42, 3316–3323, <https://doi.org/10.1021/es702253m>, 2008.
- 1007 Sciare, J., Bardouki, H., Moulin, C., and Mihalopoulos, N.: Aerosol sources and their Contribution to the chemical composition
1008 of aerosols in the Eastern Mediterranean Sea during summertime, *Atmos. Chem. Phys.*, 3, 291–302, <https://doi.org/10.5194/acp-1009-3-291-2003>, 2003.
- 1010 Sciare, J., D’Argouges, O., Zhang, Q. J., Sarda-Estève, R., Gaimoz, C., Gros, V., Beekmann, M., and Sanchez, O.: Comparison
1011 between simulated and observed chemical composition of fine aerosols in Paris (France) during springtime: Contribution of
1012 regional versus continental emissions, *Atmos. Chem. Phys.*, 10, 11987–12004, <https://doi.org/10.5194/acp-10-11987-2010>,
1013 2010.
- 1014 Siouti, E., Skyllakou, K., Kioutsioukis, I., Ciarelli, G., and Pandis, S. N.: Simulation of the cooking organic aerosol concentration
1015 variability in an urban area, *Atmos. Environ.*, 265, 118710, <https://doi.org/10.1016/j.atmosenv.2021.118710>, 2021.
- 1016 Smith, S. J., Van Aardenne, J., Klimont, Z., Andres, R. J., Volke, A., and Delgado Arias, S.: Anthropogenic sulfur dioxide
1017 emissions: 1850–2005, *Atmos. Chem. Phys.*, 11, 1101–1116, <https://doi.org/10.5194/acp-11-1101-2011>, 2011.
- 1018 Stavroulas, I., Bougiatioti, A., Grivas, G., Paraskevopoulou, D., Tsagkaraki, M., Zarnmpas, P., Liakakou, E., Gerasopoulos, E.,
1019 and Mihalopoulos, N.: Sources and processes that control the submicron organic aerosol composition in an urban Mediterranean
1020 environment (Athens): A high temporal-resolution chemical composition measurement study, *Atmos. Chem. Phys.*, 19, 901–
1021 919, <https://doi.org/10.5194/acp-19-901-2019>, 2019.
- 1022 Stavroulas, I., Grivas, G., Liakakou, E., Kalkavouras, P., Bougiatioti, A., Kaskaoutis, D. G., Lianou, M., Papoutsidaki, K.,
1023 Tsagkaraki, M., Zarnmpas, P., Gerasopoulos, E., and Mihalopoulos, N.: Online chemical characterization and sources of
1024 submicron aerosol in the major mediterranean port city of piraeus, greece, *Atmosphere (Basel)*, 12, 1–28,
1025 <https://doi.org/10.3390/atmos12121686>, 2021.



- 1026 Stein, A. F., Draxler, R. R., Rolph, G. D., Stunder, B. J. B., Cohen, M. D., and Ngan, F.: Noaa's hysplit atmospheric transport
1027 and dispersion modeling system, *Bull. Am. Meteorol. Soc.*, 96, 2059–2077, <https://doi.org/10.1175/BAMS-D-14-00110.1>, 2015.
- 1028 Sun, C., Lee, B. P., Huang, D., Jie Li, Y., Schurman, M. I., Louie, P. K. K., Luk, C., and Chan, C. K.: Continuous measurements
1029 at the urban roadside in an Asian megacity by Aerosol Chemical Speciation Monitor (ACSM): Particulate matter characteristics
1030 during fall and winter seasons in Hong Kong, *Atmos. Chem. Phys.*, 16, 1713–1728, <https://doi.org/10.5194/acp-16-1713-2016>,
1031 2016.
- 1032 Terink, W., Immerzeel, W. W., and Droogers, P.: Climate change projections of precipitation and reference evapotranspiration
1033 for the Middle East and Northern Africa until 2050, *Int. J. Climatol.*, 33, 3055–3072, <https://doi.org/10.1002/joc.3650>, 2013.
- 1034 Theodosi, C., Grivas, G., Zampas, P., Chaloulakou, A., and Mihalopoulos, N.: Mass and chemical composition of size-
1035 segregated aerosols (PM1, PM2.5, PM10) over Athens, Greece: Local versus regional sources, *Atmos. Chem. Phys.*, 11, 11895–
1036 11911, <https://doi.org/10.5194/acp-11-11895-2011>, 2011.
- 1037 Theodosi, C., Tsagkaraki, M., Zampas, P., Grivas, G., Liakakou, E., Paraskevopoulou, D., Lianou, M., Gerasopoulos, E., and
1038 Mihalopoulos, N.: Multi-year chemical composition of the fine-aerosol fraction in Athens, Greece, with emphasis on the
1039 contribution of residential heating in wintertime, *Atmos. Chem. Phys.*, 18, 14371–14391, [https://doi.org/10.5194/acp-18-14371-
1040 2018](https://doi.org/10.5194/acp-18-14371-2018), 2018.
- 1041 Tsangari, H., Paschalidou, A. K., Kassomenos, A. P., Vardoulakis, S., Heaviside, C., Georgiou, K. E., and Yamasaki, E. N.:
1042 Extreme weather and air pollution effects on cardiovascular and respiratory hospital admissions in Cyprus, *Sci. Total Environ.*,
1043 542, 247–253, <https://doi.org/10.1016/j.scitotenv.2015.10.106>, 2016.
- 1044 Ulbrich, I. M., Canagaratna, M. R., Zhang, Q., Worsnop, D. R., and Jimenez, J. L.: and Physics Interpretation of organic
1045 components from Positive Matrix Factorization of aerosol mass spectrometric data, 2891–2918, 2009.
- 1046 Vrekoussis, M., Pikridas, M., Rousogenous, C., Christodoulou, A., Desservettaz, M., Sciare, J., and Richter, A.: Science of the
1047 Total Environment Local and regional air pollution characteristics in Cyprus : A long-term trace gases observations analysis,
1048 *Sci. Total Environ.*, 845, 157315, <https://doi.org/10.1016/j.scitotenv.2022.157315>, 2022.
- 1049 Zanis, P., Hadjinicolaou, P., Pozzer, A., Tyrlis, E., Dafka, S., Mihalopoulos, N., and Lelieveld, J.: Summertime free-tropospheric
1050 ozone pool over the eastern Mediterranean / Middle East, 115–132, <https://doi.org/10.5194/acp-14-115-2014>, 2014.
- 1051 Zhang, Y., Favez, O., Canonaco, F., Liu, D., Močnik, G., Amodeo, T., Sciare, J., Prévôt, A. S. H., Gros, V., and Albinet, A.:
1052 Evidence of major secondary organic aerosol contribution to lensing effect black carbon absorption enhancement, *npj Clim.*
1053 *Atmos. Sci.*, 1, <https://doi.org/10.1038/s41612-018-0056-2>, 2018.
- 1054 Zhang, Y., Favez, O., Petit, J., Canonaco, F., Truong, F., Bonnaire, N., Crenn, V., Amodeo, T., Prévôt, A. S. H., Sciare, J., Gros,
1055 V., and Albinet, A.: Six-year source apportionment of submicron organic aerosols from near-continuous highly time-resolved
1056 measurements at SIRT A (Paris area , France), 14755–14776, 2019.
- 1057 Zittis, G., Almazroui, M., Alpert, P., Ciais, P., Cramer, W., Dahdal, Y., Fnais, M., Francis, D., Hadjinicolaou, P., Howari, F.,
1058 Jrrar, A., Kaskaoutis, D. G., Kulmala, M., Lazoglou, G., Mihalopoulos, N., Lin, X., Rudich, Y., Sciare, J., Stenichkov, G.,
1059 Xoplaki, E., and Lelieveld, J.: Climate Change and Weather Extremes in the Eastern Mediterranean and Middle East, *Rev.*
1060 *Geophys.*, 60, <https://doi.org/10.1029/2021rg000762>, 2022.